University of Louisville
ThinkIR: The University of Louisville's Institutional Repository

Electronic Theses and Dissertations

8-2019

Allee effects introduced by density dependent phenology.

Timothy James Pervenecki
University of Louisville

Follow this and additional works at: https://ir.library.louisville.edu/etd

 Part of the Applied Mathematics Commons

Recommended Citation
Pervenecki, Timothy James, "Allee effects introduced by density dependent phenology." (2019). *Electronic Theses and Dissertations.* Paper 3291.
https://doi.org/10.18297/etd/3291

This Doctoral Dissertation is brought to you for free and open access by ThinkIR: The University of Louisville's Institutional Repository. It has been accepted for inclusion in Electronic Theses and Dissertations by an authorized administrator of ThinkIR: The University of Louisville's Institutional Repository. This title appears here courtesy of the author, who has retained all other copyrights. For more information, please contact thinkir@louisville.edu.

ALLEE EFFECTS INTRODUCED BY DENSITY DEPENDENT PHENOLOGY

By

Timothy James Pervenecki
B.S., University of Southern Indiana, Indiana, USA, 2013
M.A., University of Louisville, Kentucky, USA, 2015

A Dissertation
Submitted to the Faculty of the
College of Arts and Sciences of the University of Louisville
in Partial Fulfillment of the Requirements
for the Degree of

Doctor of Philosophy
in
Industrial and Applied Mathematics

Department of Mathematics
University of Louisville
Louisville, KY

August 2019

ALLEE EFFECTS INTRODUCED BY DENSITY DEPENDENT PHENOLOGY

Submitted by

Timothy James Pervenecki

A Dissertation Approved on

June 28, 2019

by the following Dissertation Committee:

Dr. Bingtuan Li, Dissertation Director

Dr. Sarah Emery

Dr. Gung-Min Gie

Dr. Changbing Hu

Dr. David Swanson

DEDICATION

This dissertation is dedicated

to my wife Surina Borjigin and my parents, for tolerating me during this stressful time.

ACKNOWLEDGEMENTS

- This research was partially supported by the National Science Foundation under Grant DMS-1515875.
- Dr. Bingtuan Li for his guidance, encouragement, and purchasing Mathematica.
- Dr. William Fagan and Dr. Sharon Bewick for thier help with biology.
- Dr. Garrett Otto for his help with simulations.
- Sam Lord for his generous donation of the mathematics computer lab.
- Dr. Thomas Riedel for giving me after hours access to the mathematics computer lab.
- Dr. Adam Jobsom for his assistance with LaTeX typesetting issues.
- My wife, Surina Borjigin for putting up with me.
- Dr. Thomas Riedel, Dr. Robert Powers, and Dr. Ryan Gill for administrative help and academic guidance.

ABSTRACT

ALLEE EFFECTS INTRODUCED BY DENSITY DEPENDENT PHENOLOGY

Timothy James Pervenecki

June 28, 2019

We consider both the nonspatial model and spatial model of a species that gives birth to eggs at the end of the year. It is assumed that the timing of emergence from eggs is controled by phenology, which is density dependent. In general, the solution maps for our models are implicit; When the solution map is explicit, it is extremely complex and it is easier to work with the implicit map. We derive integral conditions for which the nonspatial model exhibits strong Allee effect. We also provide a necessary condition and a sufficient condition for the existence of positive equilibrium solutions. We also numerically explore the complex dynamics of both models. It is shown that varying a parameter can cause an Allee threshold to appear/disappear. We also show that the spatial model can have a growth function with overcompensation, wave solutions, oscillating waves, and nonspreading solutions. It is also shown that the wave solutions can have constant, oscillating, or chaotic spreading speeds. We also provide an example where the solutions to the spatial model are persistent, even though the underlying dynamics of the nonspatial model is essential extinction.

TABLE OF CONTENTS

CHAPTER

1. INTRODUCTION 1
2. THE NONSPATIAL MODEL 13
   2.1 THE MODEL 13
   2.2 NUMERICAL SIMULATIONS FOR MODEL (2.1) 16
      2.2.1 WHEN THE PHENOLOGY FUNCTION IS THE UNIFORM DISTRIBUTION 18
      2.2.2 WHEN THE PHENOLOGY FUNCTION IS THE GAMMA DISTRIBUTION 31
      2.2.3 WHEN THE PHENOLOGY FUNCTION IS THE GENERALIZED BETA DISTRIBUTION 36
3. THE SPATIAL MODEL 39
   3.1 THE MODEL 39
   3.2 NUMERICAL SIMULATIONS FOR MODEL (3.1) 42
      3.2.1 WHEN THE PHENOLOGY FUNCTION IS THE UNIFORM DISTRIBUTION 43
      3.2.2 WHEN THE PHENOLOGY FUNCTION IS THE GAMMA DISTRIBUTION 51
      3.2.3 WHEN THE PHENOLOGY FUNCTION IS THE GENERALIZED BETA DISTRIBUTION 55
4. CONCLUSIONS 57

REFERENCES 61

APPENDIX 65
A.1 LEMMAS 65
A.2 PROOF OF THEOREM 2.1 66
A.3 PROOF OF PROPOSITION 2.1 69
A.4 PROOF OF PROPOSITION 2.2 70
A.5 PROOF OF PROPOSITION 2.3 71
A.6 DERIVATION OF $\Lambda(\mu)$ 72
CURRICULUM VITAE 74

LIST OF FIGURES

1.1	Example of a map with the strong Allee effect	3
1.2	Example of a map with the weak Allee effect	3
2.1	How the parameters affect the uniform distribution	19
2.2	Bifurcation and Fixed Point Diagrams for $\beta \in [0.1, 0.6]$ and Growth Function for $\beta = 0.3$ with $g(P,t)$ given by Equation (2.4)	20
2.3	Bifurcation and Fixed Point Diagrams for $\beta \in [0.05, 0.3]$ and Growth Function for $\beta = 0.1$ with $g(P,t)$ given by Equation (2.4)	21
2.4	Bifurcation and Fixed Point Diagrams for $\theta \in [0, 0.2]$ and Growth Functions for $\theta = 0$ and $\theta = 0.18$ with $g(P,t)$ given by Equation (2.4)	22
2.5	Bifurcation and Fixed Point Diagrams for $\nu \in [0, 10]$ and Growth Function for $\nu = 8$ with $g(P,t)$ given by Equation (2.4)	23
2.6	Bifurcation and Fixed Point Diagrams for $\nu \in [0, 10]$ and Growth Function for $\nu = 8$ with $g(P,t)$ given by Equation (2.4)	24
2.7	Bifurcation and Fixed Point Diagrams for $\nu \in [0, 8]$ and Growth Function for $\nu = 8$ with $g(P,t)$ given by Equation (2.4)	25
2.8	Bifurcation and Fixed Point Diagrams for $\alpha \in [0, 50]$ and Growth Function for $\alpha = 17$ with $g(P,t)$ given by Equation (2.4) . . .	26
2.9	Bifurcation and Fixed Point Diagrams for $\beta \in [0, 1.1]$ and Growth Function for $\beta = 0.4$ with $g(P,t)$ given by Equation (2.4) . . .	27
2.10	Bifurcation and Fixed Point Diagrams for $\alpha \in [0, 10]$ and Growth Function for $\alpha = 2$ with $g(P,t)$ given by Equation (2.4)	28

2.11 Bifurcation and Fixed Point Diagrams for $\nu \in [0, 10]$ and Growth Function for $\nu = 1.8$ with $g(P, t)$ given by Equation (2.4) . . . 29
2.12 Bifurcation and Fixed Point Diagrams for $\alpha \in [0, 30]$ and Growth Function for $\alpha = 12$ with $g(P, t)$ given by Equation (2.4) . . . 30
2.13 How the parameters affect the gamma distribution 31
2.14 Bifurcation and Fixed Point Diagrams for $\nu \in [0, 2]$ and Growth Function for $\nu = 0.1$ with $g(P, t)$ given by Equation (2.7) . . . 32
2.15 Bifurcation and Fixed Point Diagrams for $\nu \in [0, 2]$ and Growth Function for $\nu = 1$ with $g(P, t)$ given by Equation (2.7) 33
2.16 Bifurcation and Fixed Point Diagrams for $\nu \in [0, 10]$ and Growth Function for $\nu = 5$ with $g(P, t)$ given by Equation (2.7) 34
2.17 Bifurcation and Fixed Point Diagrams for $\alpha \in [0, 35]$ and Growth Function for $\alpha = 21$ with $g(P, t)$ given by Equation (2.7) . . . 35
2.18 How the parameters affect the generalized beta distribution . . 37
2.19 Bifurcation and Fixed Point Diagrams for $\nu \in [0, 15]$ and Growth Function for $\nu = 10.5$ with $g(P, t)$ given by Equation (2.8) . . . 37
3.1 Wave Solutions with Constant Spreading Speed for Model (3.1) with $g(P, t)$ given by Equation (2.4) 43
3.2 Oscillating Wave Solutions with Constant Spreading Speed for Model (3.1) with $g(P, t)$ given by Equation (2.4) 44
3.3 Oscillating Wave Solutions with Constant Spreading Speed for Model (3.1) with $g(P, t)$ given by Equation (2.4) 45
3.4 Oscillating Wave Solutions with Constant Spreading Speed for Model (3.1) with $g(P, t)$ given by Equation (2.4) 45
3.5 Chaotic Wave Solutions with Oscillating Spreading Speed for Model (3.1) with $g(P, t)$ given by Equation (2.4) 46

3.6 Chaotic Wave Solutions with Oscillating Spreading Speed for Model (3.1) with $g(P,t)$ given by Equation (2.4) 47
3.7 Chaotic Wave Solutions with Oscillating Spreading Speed for Model (3.1) with $g(P,t)$ given by Equation (2.4) 47
3.8 Chaotic Wave Solutions with Oscillating Spreading Speed for Model (3.1) with $g(P,t)$ given by Equation (2.4) 48
3.9 Nonspreading Solution for Model (3.1) with $g(P,t)$ given by Equation (2.4) 49
3.10 Wave Solutions with Oscillating Spreading Speed for Model (3.1) with $g(P,t)$ given by Equation (2.4) 50
3.11 Nonspreading Solution for Model (3.1) with $g(P,t)$ given by Equation (2.4) 50
3.12 Wave Solution with Constant Spreading Speed for Model (3.1) with $g(P,t)$ given by Equation (2.4) 51
3.13 Wave Solutions with Constant Spreading Speed for Model (3.1) with $g(P,t)$ given by Equation (2.7) 52
3.14 Wave Solutions with Constant Spreading Speed for Model (3.1) with $g(P,t)$ given by Equation (2.7) 52
3.15 Nonspreading Solution for Model (3.1) with $g(P,t)$ given by Equation (2.7) 53
3.16 Nonspreadng Solution for Model (3.1) with $g(P,t)$ given by Equation (2.7) 54
3.17 Oscillating Wave Solutions with Chaotic Spreading Speed for Model (3.1) with $g(P,t)$ given by Equation (2.7) 54
3.18 Chaotic Wave Solutions with Chaotic Spreading Speed for Model (3.1) with $g(P,t)$ given by Equation (2.8) 55

CHAPTER 1
INTRODUCTION

Phenology (seasonal biological timing) is a topic of great interest in ecology. Phenology is studied to help understand how the timing of certain processes (such as births or transitioning to a new life stage) affects the dynamics of the system. In ecological systems, changes in phenology can involve changes in the start/end time of a process and/or changes in the synchrony of that process. Phenology plays a very important role in the study of invasive species, which is an area of great interest in applied ecology. Logan and Powell (2001), Ward and Masters (2007), and Robinet et al. (2008) have studied how phenological asynchrony affects the success of invasion for a variety of species. It was shown for the gypsy moth (*Lymantria dispar*), that a cause of asynchrony in the breeding adults was variation in the development rates of the juveniles (Robinet et al., 2007, 2008; Gascoigne et al., 2009). The asynchrony in reproduction makes it possible for some females to miss mating opportunities, which in turn can slow the spread of the species (Johnson et al., 2006; Tobin et al., 2007). Gray (2004) showed that variation in the developmental rates may be caused by genetics. It has also been shown that variation in phenological events can be caused by environmental conditions, such as temperature or elevation (Walter et al., 2015).

Ecologists regularly collect data on the begining and duration of life stages of a species. This data is well represented as a function of time, which makes it easy to model phenology with time-dependent functions. However, for several plants

such as *Phaseolus Vulgaris L.* (Abubaker, 2008) and the cleistogamous flowers of *Impatiens capensis* (Schmitt et al., 1987), it has been shown that low (high) densities can delay (advance) flowering. It is also possible that low (high) densities can advance (delay) flowering for the chasmogamous flowers of *Impatiens capensis* (Schmitt et al., 1987), but this result was not statistically significant due to a small sample size. Due to the fact that population density can effect phenology, we switch from modeling phenology as purely time-dependent to modeling phenology as both time- and density-dependent.

A *demographic Allee effect* is the positive relationship between the overall individual fitness (often measured in per capita growth rate) and population density (`https://en.wikipedia.org/wiki/Allee_effect`). A demographic Allee effect can be subdivided into two categories, strong Allee effect and weak Allee effect. For an Allee effect to be strong, there must exist a density threshold that must be overcome for the species to survive. An example of a discrete map with the strong Allee effect can be seen below.

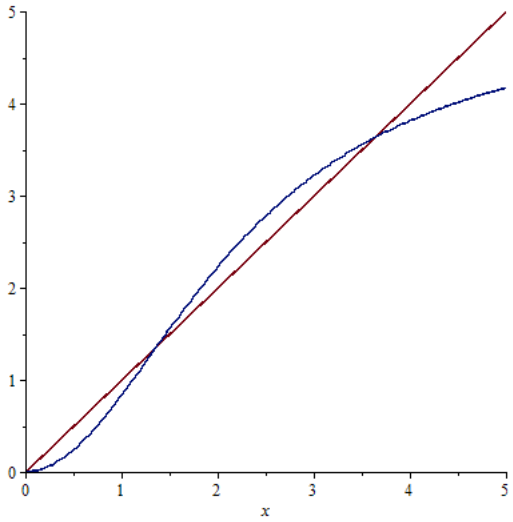

$$f(x) = \frac{5x^2}{5 + x^2}$$

Figure 1.1: Example of a map with the strong Allee effect

For an Allee effect to be weak, there must be no density threshold that must be overcome for the species to survive.

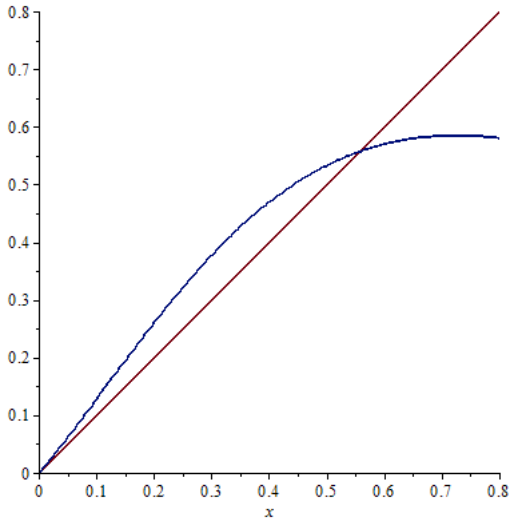

$$f(x) = xe^{2(1-x-\frac{3.75}{4+8x})}$$

Figure 1.2: Example of a map with the weak Allee effect

The goal of this dissertation is to show that density dependent phenology can cause the Allee effect. This is a previously undiscovered mechanism for generating the Allee effect.

In Chapter 2.1, we define the biological and mathematical assumptions that we impose on our main model. The structure of the model, the with-in season dynamics are governed by an ordinary-differential equation and the between-season dynamics are governed by a multiple of the population that survives to the end

of the season ($t = 1$) is the initial population for the following season, follows the structure of the models in Eskola and Parvinen (2007, 2010) (discussed below). The assumptions that we make lead to a nonautonomus scalar model that does not have an explicit stage structure. The model assumes that the population growth is controlled by phenology, which is density-dependent. The model is highly nonlinear and in general, can not be explicitly solved. We provide a theorem for the existence of the Allee effect and if the Allee effect is present, we provide a condition for the Allee effect to be strong. It is shown that when the Allee effect is present, that it is caused by the density-dependent phenology. We also provide a necessary condition and a sufficient condition for the existence of positive equilibrium for the model. The proofs for all of the results are located in the Appendix. One thing that stands out about our models is that we are able to generate the Allee effect with only one equation. Most mechanistic models with the Allee effect use at least two equations to generate the Allee effect. The mechanism producing the Allee effect in these models is usually mate finding (e.g., Eskola and Parvinen 2010, 2007; Berec et al. 2007; Courchamp et al. 2008; Boukal and Berec 2002). Some other mechanisms that produce the Allee effect are group defense, group feeding, and habitat alteration (e.g., Eskola and Parvinen 2007; Courchamp et al. 2002, 2008; Rinella et al. 2012).

With all the possible mechanisms that can cause the Allee effect, a large portion of the literature is devoted to studying mate finding as the mechanism generating the Allee effect (e.g., Eskola and Parvinen 2010; Boukal and Berec 2002). Several examples for mechanistic models where the Allee effect is generated by mate finding processes can be found in Eskola and Parvinen (2010) (see models (7), (25), (31), (42), and (48)) and Eskola and Parvinen (2007) (see models (11) and (18)).

In all of the models in Eskola and Parvinen (2010), it is assumed that adults and juveniles suffer from natural death at rates μ and λ, respectively; adults suffer from competition with other adults at a rate γ; juveniles suffer from competition between adults and other juveniles at rates β and δ, respectively. Eskola and Parvinen use $U(t)$ and $v(t)$ to denote the adult and juvenile densities, respectively, and x_n to denote the initial adult density in the n^{th} year. At the end of the year, $t = 1$, it is assumed that the adults die, and the juveniles that survive the winter become adults at the begining of the following year. The fraction of the juveniles that survive the winter is denoted by σ.

In models (7) and (25) in Eskola and Parvinen (2010), it is assumed that reproduction happens continuously and that the adult population consists of two sexes, females F and males M. It is also assumed that ratio of males to females remains constant across years. The fraction of the adult population that are female is denoted by s and the fraction of the adult population that are males is denoted by $1 - s$. In their model (7), it is assumed that reproduction is a result of interactions between males and females. In models (25) and (31) in Eskola and Parvinen (2010) it is further assumed that the interaction between males and females produce fertilized females ,F^*, and then the fertilized females give birth to juveniles. In model (31) it is assumed that birth is impulsive at time $T \in (0, 1]$ (i.e., birth is modeled with a δ-peak at time T, $v(T) = AF^*(T)$).

The population dynamics for model (7) in Eskola and Parvinen (2010) are governed by

$$
\begin{aligned}
&\dot{F} = -\gamma F^2 - \gamma FM - \mu F, && F(0) = sx_n,\\
&\dot{M} = -\gamma M^2 - \gamma FM - \mu M, && M(0) = (1-s)x_n,\\
&\dot{v} = \alpha FM - \beta v(F+M) - \delta v^2 - \lambda v, && v(0) = 0,\\
&x_{n+1} = \sigma v(1).
\end{aligned}
$$

The population dynamics for model (25) in Eskola and Parvinen (2010) are governed by

$$
\begin{aligned}
&\dot{F} = -\rho FM, && F(0) = sx_n,\\
&\dot{F}^* = \rho FM, && F^*(0) = 0,\\
&\dot{M} = 0, && M(0) = (1-s)x_n,\\
&\dot{v} = \alpha F^* - \beta v(F+M+F^*) - \delta v^2 - \lambda v, && v(0) = 0,\\
&x_{n+1} = \sigma v(1).
\end{aligned}
$$

The population dynamics for model (31) in Eskola and Parvinen (2010) are governed by

$$
\begin{aligned}
&\dot{F} = -\rho_T FM, && F(0) = sx_n,\\
&\dot{F}^* = \rho_T FM, && F^*(0) = 0,\\
&\dot{M} = 0, && M(0) = (1-s)x_n,\\
&\dot{v} = -\beta v(F+M+F^*) - \delta v^2 - \lambda v, && v(0) = 0 \text{ for } 0 \le t < T,\ v(T) = AF^*(T),\\
&x_{n+1} = \sigma v(1).
\end{aligned}
$$

Where

$$\rho_T = \begin{cases} \rho, & 0 \leq t < T, \\ 0, & t \geq T \end{cases}$$

In all three of these models, it is the mating function, FM, that is responsible for generating the Allee effect. More details about models (7), (25), and (31) and the proofs that theses models have the strong Allee effect can be found in Eskola and Parvinen (2010).

In models (42) and (48) in Eskola and Parvinen (2010) it is assumed that the species is isogamous (males and females are indistinguishable). It is also assumed that adults search for mates at a rate c. When a mate is found, they form a pair P. Reproduction is caused by the pair formation and can happen continuously at a rate α (model (42)) or impulsively at time $T \in (0, 1]$ (model (48)). There is no competition between paired adults and other adults. Juveniles suffer from competition with single adults but not paired adults.

The population dynamics for model (42) in Eskola and Parvinen (2010) are governed by

$$\begin{aligned} \dot{U} &= -(\gamma + c)U^2 - \mu U, & U(0) &= x_n, \\ \dot{P} &= \frac{1}{2}cU^2, & P(0) &= 0, \\ \dot{v} &= \alpha P - \beta v U - \delta v^2 - \lambda v, & v(0) &= 0, \\ x_{n+1} &= \sigma v(1). \end{aligned}$$

The population dynamics for model (48) in Eskola and Parvinen (2010) are governed by

$$\dot{U} = -(\gamma + c_T)U^2 - \mu U, \quad U(0) = x_n,$$
$$\dot{P} = \frac{1}{2}c_T U^2, \qquad\qquad P(0) = 0,$$
$$\dot{v} = -\beta v U - \delta v^2 - \lambda v, \qquad v(0) = 0 \text{ for } 0 \leq t < T, \;\; v(T) = AP(T)$$

Where

$$c_T = \begin{cases} c, & 0 \leq t < T, \\ 0, & t \geq T. \end{cases}$$

In both of these models it is the reproduction by pair formation that generates the Allee effect. More details models (42) and (48) and the proofs that models have the strong Allee effect can be found in Eskola and Parvinen (2010).

Eskola and Parvinen (2007) consider resource-consumer models with different mate finding mechanisms. All of the models that they consider they use $R_n(t)$ for the resource population (which they assume is at a quasi-equilibrium throughout the year), $x_n(t)$ for the consumer population, and $E_n(t)$ for the egg population. They assume that consumers harvest the resource at a rate β and they assume that the consumers produce eggs at a rate γ which is proportional to the food intake. It is also assumed that all of the adults (consumers) die at the end of the year ($t = 1$) and that the population at the begining of the next year is the portion of eggs that survive to the next year.

In model (11) in Eskola and Parvinen (2007), it is assumed that the consumer population consist of two sexes, males (M) and females (F), and the consumer population is given by $x_n(t) = F_n(t) + M_n(t)$. The within-season population dynamics

for model (11) are governed by

$$\dot{R}_n(t) = \alpha R_n(t) f(R_n(t)) - R_n(t)\beta(F_n(t) + M_n(t))$$
$$\dot{E}_n(t) = \gamma F_n(t) p(M_n(t))\beta R_n(t) - \delta E_n(t) - kE_n(t)(F_n(t) + M_n(t))$$
$$\dot{F}_n(t) = 0$$
$$\dot{M}_n(t) = 0$$

and the between-season dynamics are

$$R_{n+1}(0) = \rho R_n(1)$$
$$E_{n+1}(0) = 0$$
$$F_{n+1}(0) = s\sigma E_n(1) = s x_{n+1}(0)$$
$$M_{n+1}(0) = (1-s)\sigma E_n(1) = (1-s)\sigma x_{n+1}(0).$$

For this model, it is the maiting function $Fp(M)$ that generates the Allee effect. More details on model (11) and the proof that the model has the Allee effect can be found in Eskola and Parvinen (2007).

In model (18) in Eskola and Parvinen (2007), it is assumed that the species is isogamous (males and females can not be distinguished), adults (U) search for mates at a rate c, and form a pair (P), and that pairs of adults produce eggs. The within-season population dynamics for model (18) are governed by

$$\dot{R}_n(t) = \alpha R_n(t) f(R_n(t)) - R_n(t)\beta(U_n(t) + 2P_n(t))$$
$$\dot{E}_n(t) = \gamma P_n(t)\beta R_n(t) - kU_n(t)E_n(t)$$
$$\dot{U}_n(t) = -cU_n(t)^2$$
$$\dot{P}_n(t) = \frac{1}{2}cU_n(t)^2$$

and the between-season dynamics are

$$R_{n+1}(0) = \rho R_n(1)$$

$$E_{n+1}(0) = 0$$

$$U_{n+1}(0) = s\sigma E_n(1)$$

$$P_{n+1}(0) = 0.$$

For this model, it is the pair formation that generates the Allee effect. More detatils on model (18) and the proof that the model has the Allee effect can be found in Eskola and Parvinen (2007).

In Section 2.2 we investigate the dynamics of the main model for different phenology functions. We first investigate the phenology function being the uniform distribution (Section 2.2.1), the simpliest distribution we consider. For the uniform distribution (equation (2.4)), we are able to explicitly solve for the year-to-year mapping and numerically show that the mapping can be monotone (Figures 2.2 (c) and 2.12 (c)), or can have overcompensation and a cusp (Figures 2.3 (c), 2.4 (c) and (d), 2.5 (c), 2.6 (c), 2.7 (c), 2.8 (c), 2.9 (c), 2.10 (c), and 2.11 (c)). We also numerically explore how varying a parameter can effect the the dynamics of the model (Figures 2.2 (a), 2.3 (a), 2.4 (a), 2.5 (a), 2.6 (a), 2.7 (a), 2.8 (a), 2.9 (a), 2.10 (a), 2.11 (a), 2.12 (a)) and can effect the equilibrium points, i.e., causing the existence of the carrying capacity or the Allee threshold to change or increasing/decreasing the magnitude of the carrying capacity or the Allee threshold (Figures 2.2 (b), 2.3 (b), 2.4 (b), 2.5 (b), 2.6 (b), 2.7 (b), 2.8 (b), 2.9 (b), 2.10 (b), 2.11 (b), 2.12 (b)).

We then investigate the phenology function being the gamma distribution (Section 2.2.2). We numerically show that the model can have a monotone growth function (Figures 2.14 (c) and 2.15 (c)) or a smooth growth function with overcompensation (Figures 2.16 (c) and 2.17 (c)). We also numerically explore how varying a

parameter can effect the the dynamics of the model (Figures 2.14 (a), 2.15 (a), 2.16 (a), and 2.17 (a)) and can effect the equilibrium points, i.e., causing the existence of the carrying capacity or the Allee threshold to change or increasing/decreasing the magnitude of the carrying capacity or the Allee threshold (Figures 2.14 (b), 2.15 (b), 2.16 (b), and 2.17 (b)).

In Section 2.2.3, we investigate the phenology function being the generalized beta distribution (equation (2.8)). We numerically show that the model can have a growth function with overcompensation and a cusp (Figure 2.19 (c)). We also numerically explored how varying a parameter effected the dynamics of model (2.1) (Figure 2.19 (a)), can cause an Allee threshold to come into existence, and change the magnitude of the carrying capacity and Allee threshold (Figure 2.19 (b)).

In Chapter 3.1, we further develop model (2.1) by considering movement. It is assumed that adults move according to random diffusion processes. This gives a new model where the dynamics are governed by a reaction-diffusion equation. For this model, we provide a theorem on the existence of a positive unique solution. If the assumption that phenology is density dependedt is removed, the model becomes a special case of the model discussed by Otto et al. (2018). In Section 3.2, we investigate this spatial model spatial model when the phenology function is given by the uniform distribution (Section 3.2.1), the gamma distribution (Section 3.2.2), and the generalized beta distribution (Section 3.2.3). When discussing solutions to our spatial model, we call a nonnegative solution (that is not identically zero) that spreads in both directions a wave solution. If the wave solution oscillates, and the oscillations appear to follow a pattern, it is called an oscillating wave solution. If the wave solution oscillates, and the oscillations do not appear to follow a pattern, it is called a chaotic wave solution. When the phenology function is the uniform

distribution (equation (2.4)) we numerically show that the model can exhibit wave (Figures 3.1 (a), 3.10 (a), and 3.12 (a)), oscillating wave (Figures 3.2 (a), 3.3 (a), and 3.4 (a)), chaotic wave (Figures 3.5 (a), 3.6 (a), 3.7 (a), and 3.8 (a)), and nonspreading solutions (Figures 3.9 (a) and 3.11 (a)). We also show that these solutions can spread with a constant (Figures 3.1 (b), 3.2 (b), 3.3 (b), 3.4 (b), and 3.12 (b)) or oscillating (Figures 3.5 (b), 3.6 (b), 3.7 (b), 3.8 (b), and 3.10 (b)) spreading speeds. When the phenology function is the gamma distribution (equation (2.7)) we numerically show that the model can exhibit wave (Figures 3.13 (a) and 3.14 (a)), oscillating wave (Figure 3.17 (a)), and nonspreading (Figures 3.15 (a) and 3.16 (a)). We also show that these solutions can spread with constant (Figures 3.13 (b) and 3.14 (b)) or chaotic (Figure 3.17 (b)) spreading speeds. When the phenology function is the generalized beta distribution (equation (2.8)) we numerically show that the model can exhibit chaotic wave solutions (Figure 3.18 (a)) that spreads with a chaotic spreading speed (Figure 3.18 (b)).

CHAPTER 2
THE NONSPATIAL MODEL

2.1 THE MODEL

We consider a hybrid dynamical model (Mailleret and Lemesle, 2009; Lewis and Li, 2012; Otto et al., 2018) of an annual species. The within season adult density is denoted by $A(P,t)$ for $t \in [0,1]$ and P_n denotes the initial density of eggs (or seeds) at the begining of the n^{th} year. We consider a population that suffers from natural death at a rate ν and assume that competition between adults is quadratic with coefficient β. The emergence of adults is controlled by phenology, which is density dependent. The phenology kernel is denoted by $g(P,t)$. At the end of the season, adults give birth to eggs (or produce seeds) and then die and any juveniles that have not emmerged into adults by this time also die. The average number of offspring per adult that survive the winter is α. The season ends at time $t = 1$ after the adults have given birth. The population dynamics are governed by

$$\begin{aligned} A_t &= \alpha g(P_n,t)P_n - \nu A - \beta A^2, \quad A(P_n,0) = 0 \\ P_{n+1} &= A(P_n,1). \end{aligned} \tag{2.1}$$

Model (2.1) can also be used to model a few other biological scenarios. One scenario is an annual species with continuous reproduction within the year and an implicit juvenile stage that occurs during the winter. For such a case, we assume

that α $(0 < \alpha < 1)$ is the fraction of the population that survives the winter to emerge the following year and $-\nu$ $(\nu < 0)$ is the intrinsic growth rate of the population. Another scenario is a non-annual species that hibernates during the winter. For this case, α $(0 < \alpha \leq 1)$ is the fraction of the population that survives the winter; $-\nu$ $(\nu < 0)$ is the intrinsic growth rate of the population; and it is assumed that there is no interaction between hibernating adults and adults that have emerged from hibernation.

We make the following hypotheses on model (2.1).

HYPOTHESES 2.1.

i. α *and* β *are positive numbers, and* ν *is a real number.*

ii. For all $P, t \geq 0$, $g(P,t)$ *is defined,* $g(P,t) \geq 0$ *and* $\int_0^\infty g(P,t)dt = 1$.

iii. $\frac{\partial}{\partial P} g(P,t)\Big|_{P=0}$ *is defined for all but a finite number of points.*

Assuming Hypotheses 2.1 are satisfied, solutions to model (2.1) are of the form $x_{n+1} = f(x_n)$. In general the function f is implicit; when f is explicit, it is very complicated and difficult to work with. It is known that a discrete-time model of the form $x_{n+1} = f(x_n)$ has the Allee effect if $f''(0) > 0$ and that the Allee effect is strong (i.e., an extinction threshold exists, refered to as an Allee threshold) if $f'(0) < 1$ (e.g. Eskola and Parvinen 2010; Berec et al. 2007). This leads to the following theorem regarding the existence of the Allee effect for model (2.1).

THEOREM 2.1. *Assume that Hypotheses 2.1 are satisfied. Then model* (2.1) *has Allee effect if*

$$\int_0^1 \left(\left[\frac{\partial}{\partial P} g(P,t) \right] \Big|_{P=0} \right) e^{-(1-t)\nu} dt > \alpha\beta \int_0^1 g(0,t) e^{-(1-t)\nu} \int_t^1 e^{-\nu s} \int_0^s g(0,r) e^{\nu r} dr ds dt \tag{2.2}$$

In addition, the Allee effect is strong if

$$\alpha \int_0^1 g(0;t) e^{-(1-t)\nu} dt < 1. \tag{2.3}$$

The proof for Theorem 2.1 is provided in the appendix.

Condition (2.2) comes from the property that the second derivative of the solution map evaluated at $P = 0$ is positive (i.e., the solution map is concave up in a neighborhood of 0). One consequence of condition (2.2) is that if the upper bound of the support of $g(P,t)$ is larger than 1, then it is easier to have Allee effect (i.e., having only a portion of the eggs, that survived the winter, hatch can make it easier for a species to have the Allee effect). Condition (2.3) comes from the derivative of the solution map evaluated at $P = 0$. When condition (2.3) is satisfied, we have the trivial solution, $P = 0$, is stable (i.e., it is impossible for a species to persist with an initial condition near zero). When both conditions (2.2) and (2.3) are satisfied, the solution map is concave up (in a neighborhood of 0) with the trivial solution stable (i.e., model (2.1) has both Allee effect and an extinction threshold that must be overcome for survival of the species).

COROLLARY 2.1. *When model* (2.1) *has the Allee effect, it is caused by the density-dependent phenology.*

Note that the right hand side of condition (2.2) is always positive. If the phenology function is not density dependent, than the left hand side of condition (2.2) would be 0 and hence the condition would not be satisfied.

PROPOSITION 2.1. *Assume that Hypotheses* (2.1) *are satisfied and* $\nu \geq 0$. *Then a necessary condition for the existence of a positive equilibrium in model* (2.1) *is* $\alpha \geq 1$ *and that there exist* $P > 0$ *such that* $\alpha \int_0^1 g(P,t)e^{-(1-t)\nu}dt \geq 1$.

PROPOSITION 2.2. *Assume that Hypotheses 2.1 are satisfied. Furthermore, assume that model* (2.1) *has the strong Allee effect. Then a sufficient condition for the existence of a positive equilibrium is that there exists* $P > 0$ *such that*

$$\alpha g(P,t) - \beta P - \nu > 0$$

for all $0 \leq t \leq 1$, *and*

$$\int_0^1 (\alpha g(P,s) - \beta P)e^{-\nu(1-s)}ds > 1.$$

The proofs for the propositions are located in the appendix.

A necessary condition for Proposition 2.2 to be satisfied is that $[0,1]$ is a subset of the support of $g(P,t)$. In Section 2.2, there are several simulations that satisfy Proposition 2.2 (e.g., Figures 2.2 (c), 2.3 (c), 2.4 (c), and 2.15 (c)) and several that fail Proposition 2.2 but still have a positive equilibrium (e.g., Figures 2.4 (d), 2.7 (c), 2.10 (c), 2.11 (c), and 2.12 (c)).

2.2 NUMERICAL SIMULATIONS FOR MODEL (2.1)

In this section we will investigate the rich dynamics of model (2.1) when the phenological functions are the uniform distribution (Figures 2.2, 2.3, 2.4, 2.5, 2.6, 2.7, 2.8, 2.9, 2.10, 2.11, and 2.12), gamma distribution (Figures 2.14, 2.15, 2.16, and 2.17), and the generalized beta distribution (Figure 2.19). We show that density-dependent phenology can produce both the Allee effect with a monotone growth

function (see Figures 2.2 (c), 2.12 (c), 2.14 (c), and 2.15 (c)) and the Allee effect with overcompensation, a growth function that is increasing on an interval $(0, a)$ and decreasing on the interval (a, ∞) for some $a > 0$, (see Figures 2.3 (c), 2.4 (c), 2.5 (c), 2.6 (c), 2.7 (c), 2.8 (c), 2.9 (c), 2.10 (c), 2.11 (c), 2.16 (c), 2.17 (c), and 2.19 (d)). We also investigate how varying the parameters in model (2.1) affect the dynamics of the model and change equilibrium solutions (Figures 2.2 (b), 2.3 (b), 2.4 (b), 2.5 (b), 2.6 (b), 2.7 (b), 2.8 (b), 2.9 (b), 2.10 (b), 2.11 (b), 2.12 (b), 2.14 (b), 2.15 (b), 2.16 (b), 2.17 (b), and 2.19 (b)).

Recall that low (high) densities can delay (advance) the starting time of emergence and increase the duration of emergence (Abubaker, 2008; Schmitt et al., 1987) and that is also possible that low (high) densities can advance (delay) the start of phenological events. To account for this, we assume that the density-dependent parameters of the phenological function are either nonincreasing or nondecreasing. For the bifurcation diagram, we start by fixing all but one parameter in the model, the parameter that is not fixed (called the bifurcation parameter) is given a lower, bound bif_min, an upper bound, bif_max, and a step size (step) is set. We also need two parameters for ploting, N_ignore (the number of generations to ignore) and N_plot (the number of generations to plot). N_ignore is usually set around 700 or 800 to allow the dynamics to settle down. To create the bifurcation diagram, we (numerically) recursively solve model (2.1) N_ignore+N_plot times, then we plot the last N_plot solutions. Next we move the bifurcation parameter to bif_min+step and repeat this process. This is repeated until the bifurcation parameter reaches bif_max. Similarly, for the fixed point diagrams, we start by fixing all but one parameter in the model, the parameter that is not fixed (called the bifurcation parameter) is given a lower, bound bif_min, an upper bound, bif_max, and a step size (step_bif) is set. We also need to set a range for the population size that is

being examined. We let the lower bound of the population size be p_min and the upper bound be p_max. We also set a step size (step_p) and a threshold $\gamma > 0$ (used to test if a value is a fixed point). To create the fixed point diagram we start with the bifurcation parameter at bif_min and the population parameter at p_min. We then numerically solve model (2.1) and test the condition $|P_{n+1} - P_n| < \gamma$. If the condition is satisfied we plot a point, if it is not satisfied we do nothing. Then we move the population parameter to p_min+step_p, numerically solve the model, and check if the condition is met. We repeat this process until the population parameter reaches p_max. Then we move the bifurcation parameter to bif_min+step_bif and repeat the previous process until the bifurcation parameter reaches bif_max. For the growth function diagram we fix all of the parameters and set a range for the population size that is being examined. We let the lower bound of the population size be p_min and the upper bound be p_max. We also define a step size (step) used to move from p_min to p_max. To create the growth function diagram, we start at p_min, numerically solve model (2.1), and plot the solution. Then we move to p_min+step, numerically solve the model, and plot the solution. This process is repeated until we reach p_max.

2.2.1 WHEN THE PHENOLOGY FUNCTION IS THE UNIFORM DISTRIBUTION

Consider the uniform distribution given by:

$$g(P,t) = \begin{cases} \dfrac{1}{k(P) - \theta(P)} & \text{, if } \theta(P) \leq t \leq k(P_n) \\ 0 & \text{, otherwise} \end{cases} \tag{2.4}$$

It is assumed that $0 \leq \theta(P) < k(P)$, $\forall P \geq 0$. For the uniform distribution,

$\theta(P)$ indicates the time that emergence begins and $k(P)$ indicates the time that emergence ends. How these parameters affect the uniform distribution can be seen in Figure 2.1.

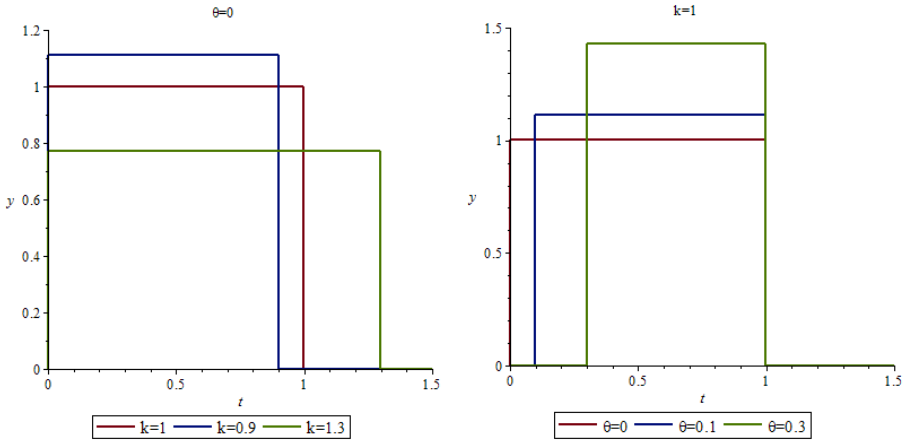

(a) $g(P,t)$ for different values of k with θ fixed (b) $g(P,t)$ for different values of θ with k fixed

Figure 2.1: How the parameters affect the uniform distribution

Since the uniform distribution is piecewise constant, we can solve model (2.1) and get an explicit year-to-year map for the population. The year-to-year map $P_{n+1} = f(P_n)$ is given in the following proposition.

PROPOSITION 2.3. *If the phenology function, $g(P,t)$, is given by the uniform distribution (equation (2.4)), then the year-to-year mapping $P_{n+1} = f(P_n)$ is given by*

$$f(P) = \begin{cases} h(1) & 1 \le k(P) \\ \dfrac{\nu h(k(P))e^{\nu k(P)}}{(\nu + \beta h(k(P)))e^{\nu} - \beta h(k(P))e^{\nu k(P)}} & k(P) < 1 \end{cases} \tag{2.5}$$

where

$$h(t) = \frac{\frac{\nu}{2\beta} + \frac{J(P)\tanh\left(\frac{1}{2}\left(\frac{t-\theta(P)}{k(P)-\theta(P)}\right)J(P)\right)}{2\beta(k(P)-\theta(P))}}{1 + \frac{\nu(k(P)-\theta(P))}{J(P)}\tanh\left(\frac{1}{2}\left(\frac{t-\theta(P)}{k(P)-\theta(P)}\right)J(P)\right)} + \frac{\nu}{2\beta} \tag{2.6}$$

where

$$J(P) = \sqrt{(k(P)-\theta(P))(\nu^2(k(P)-\theta(P)) + 4\alpha\beta P)}.$$

The proof for the proposition is located in the appendix.

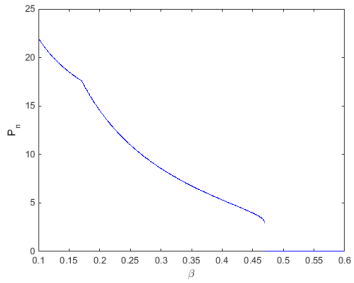

(a) Attracting Solutions for model (2.1) with $\beta \in [0.1, 0.6]$ and $P_0 = 3$

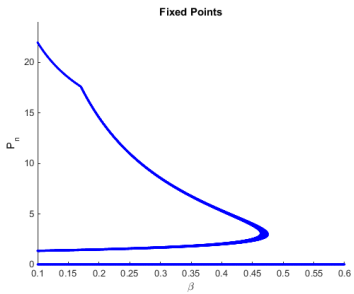

(b) Fixed Points for model (2.1) with $\beta \in [0.1, 0.6]$

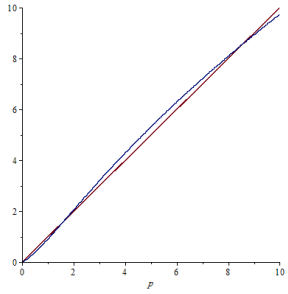

(c) Numerical Approximation of the Growth Function for model (2.1) with $\beta = 0.3$

$\theta(P) = 0$, $k(P) = 3.2 - \frac{2.25P}{0.4+P}$, $\alpha = 9$, $\nu = 6$, $\beta \in [0.1, 0.6]$

Figure 2.2: Bifurcation and Fixed Point Diagrams for $\beta \in [0.1, 0.6]$ and Growth Function for $\beta = 0.3$ with $g(P, t)$ given by Equation (2.4)

Consider model (2.1) with the phenology function, $g(P, t)$, as defined in equation (2.4) and parameters $\theta(P) = 0$, $k(P) = 3.2 - \frac{2.25P}{0.4+P}$, $\alpha = 9$, $\nu = 6$, and $\beta \in [0.1, 0.6]$. We see that increasing β (the rate of competition between adults) decreases the carrying capacity of the species (Figure 2.2 (a) and (b)) while simultaneously increasing the Allee threshold (Figure 2.2 (b)). With $\beta \approx 0.455$, the the carrying capacity and the Allee threshold meet and disappear, and the species becomes extinct. If we let $\beta = 0.3$, we see that model (2.1) has a monotone growth function and the strong Allee effect (Figure 2.2 (c)).

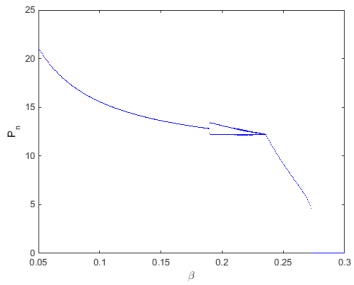

(a) Attracting Solutions for model (2.1) with $\beta \in [0.05, 0.3]$ and $P_0 = 9$

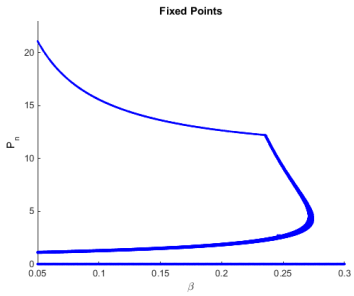

(b) Fixed Points for model (2.1) with $\beta \in [0.05, 0.3]$

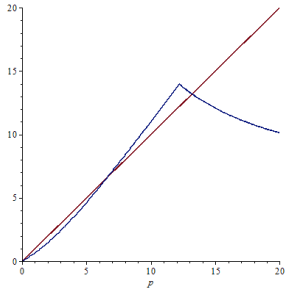

(c) Numerical Approximation of the Growth Function for model (2.1) with $\beta = 0.1$

$\theta(P) = 0$, $k(P) = 3.2 - \frac{3.1P}{5+P}$, $\alpha = 3.4$, $\nu = 1.5$, $\beta \in [0.05, 0.3]$

Figure 2.3: Bifurcation and Fixed Point Diagrams for $\beta \in [0.05, 0.3]$ and Growth Function for $\beta = 0.1$ with $g(P, t)$ given by Equation (2.4)

Consider model (2.1) with the phenology function, $g(P, t)$, as defined in equation (2.4) and parameters $\theta(P) = 0$, $k(P) = 3.2 - \frac{3.1P}{5+P}$, $\alpha = 3.4$, $\nu = 1.5$, and $\beta \in [0.05, 0.3]$. We see that increasing β (the rate of competition between adults) decreases the carrying capacity of the species, while simultaneously increasing the Allee threshold (Figure 2.3 (a) and (b)). When $\beta \approx 0.19$ the stable solution bifurcates into a period two solution until $\beta \approx 0.24$ when the solution goes through period undoubling back to a period one solution. When $\beta \approx 0.28$ the stable solution abruptly jumps to the trivial solution (Figure 2.3 (a)) due to the carrying capacity and Allee threshold intersecting and disappearing (Figure 2.3 (b)). If we let $\beta = 0.1$, we see that model (2.1) has the strong Allee effect and has a growth function with overcompensation and a cusp (Figure 2.3 (c)).

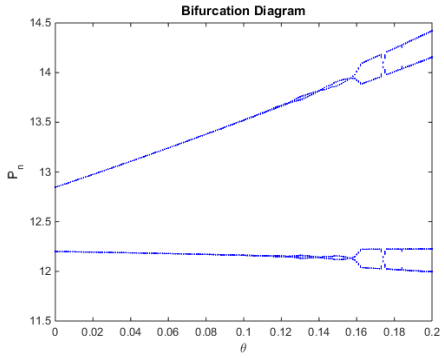

(a) Attracting Solutions for model (2.1) with $\theta \in [0, 0.2]$ and $P_0 = 3$

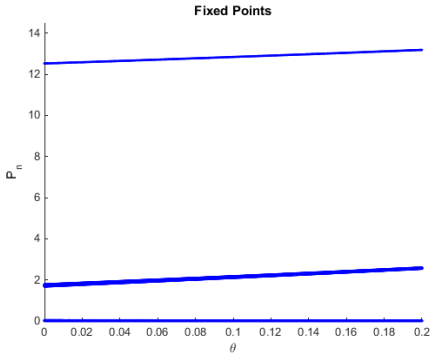

(b) Fixed Points for model (2.1) with $\theta \in [0, 0.2]$

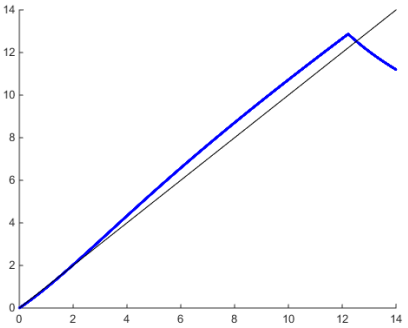

(c) Numerical Approximation of the Growth Function for model (2.1) with $\theta = 0$

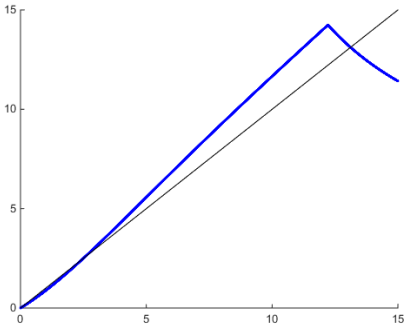

(d) Numerical Approximation of the Growth Function for model (2.1) with $\theta = 0.18$

$\theta \in [0, 0.2]$, $k(P) = 3.2 - \frac{3.1P}{5+P}$, $\alpha = 3.3$, $\nu = 0.4$, $\beta = 0.21$

Figure 2.4: Bifurcation and Fixed Point Diagrams for $\theta \in [0, 0.2]$ and Growth Functions for $\theta = 0$ and $\theta = 0.18$ with $g(P, t)$ given by Equation (2.4)

Consider model (2.1) with the phenology function, $g(P, t)$, as defined in equation (2.4) and parameters $\theta \in [0, 0.2]$, $k(P) = 3.2 - \frac{3.1P}{5+P}$, $\alpha = 3.3$, $\nu = 0.4$, and $\beta = 0.21$. We see that increasing θ (the starting time of emergence) increases the amplitude of oscillation of the periodic solution (Figure 2.4 (a)) and increases both the carrying capacity and the Allee threshold (Figure 2.4 (b)). When $\theta \approx 0.16$ the solution goes through period doubling bifurcation into a period four solution

(Figure 2.4 (a)). If we let $\theta = 0$, we see that model (2.1) has the strong Allee effect and has a growth function with overcompensation and a cusp (Figure 2.4 (c)). If we let $\theta = 0.18$, we see that model (2.1) has the strong Allee effect and has a growth function with overcompensation and a cusp (Figure 2.4 (d)).

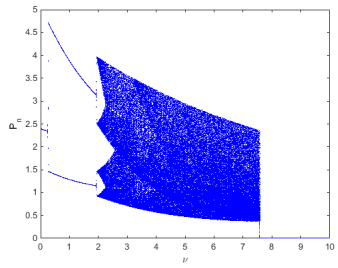

(a) Attracting Solutions for model (2.1) with $\nu \in [0, 10]$ and $P_0 = 1$

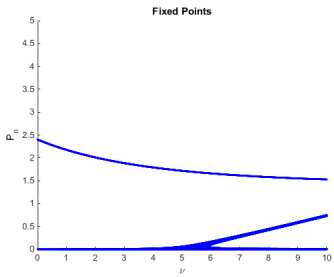

(b) Fixed Points for model (2.1) with $\nu \in [0, 10]$

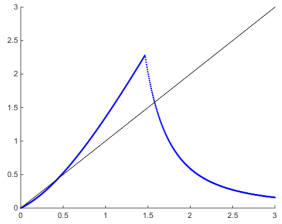

(c) Numerical Approximation of the Growth Function for model (2.1) with $\nu = 8$

$\theta(P) = 0$, $k(P) = 3.2 - \frac{3.1P}{0.6+P}$, $\alpha = 16$, $\nu \in [0, 10]$, $\beta = 1$

Figure 2.5: Bifurcation and Fixed Point Diagrams for $\nu \in [0, 10]$ and Growth Function for $\nu = 8$ with $g(P, t)$ given by Equation (2.4)

Consider model (2.1) with the phenology function, $g(P, t)$, as defined in equation (2.4) and parameters $\theta(P) = 0$, $k(P) = 3.2 - \frac{3.1P}{0.6+P}$, $\alpha = 16$, $\nu \in [0, 10]$, and $\beta = 1$. We see that increasing ν (the rate of natural death) the solution goes through period doubling bifurcation for $\nu \approx 0.2$ and shrinks the oscillation of the periodic solution; the solution becomes chaotic around $\nu \approx 2$, continuing to increase ν causes the oscillations to decrease; when $\nu \approx 7.6$ the dynamics change to essential extinction (Figure 2.5 (a)). In Figure 2.5 (b), we see that increasing ν decreases the carrying capacity of the species; for $\nu \in [0, \psi]$, $\psi \approx 5.5$, the only positive solution is the carrying capacity, with $\nu \approx 5.5$ an Allee threshold comes into existance and the Allee threshold increases as ν increases. If we let $\nu = 8$, we see that model (2.1) has the strong Allee effect and has a growth function with overcompensation and a

cusp (Figure 2.5 (c)).

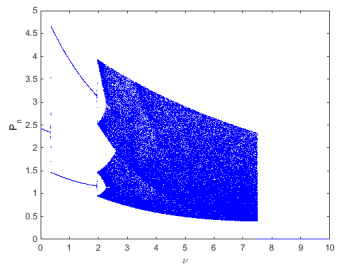

(a) Attracting Solutions for model (2.1) with $\nu \in [0, 10]$ and $P_0 = 1$

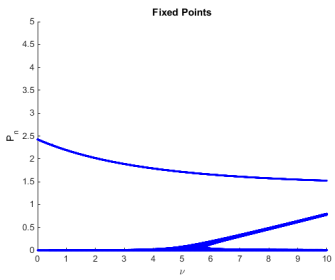

(b) Fixed Points for model (2.1) with $\nu \in [0, 10]$

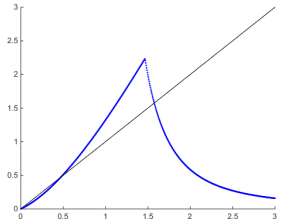

(c) Numerical Approximation of the Growth Function for model (2.1) with $\nu = 8$

$\theta(P) = 0$, $k(P) = 3.2 - \frac{3.1P}{0.6+P}$, $\alpha = 15.5$, $\nu \in [0, 10]$, $\beta = 0.97$

Figure 2.6: Bifurcation and Fixed Point Diagrams for $\nu \in [0, 10]$ and Growth Function for $\nu = 8$ with $g(P, t)$ given by Equation (2.4)

Consider model (2.1) with the phenology function, $g(P, t)$, as defined in equation (2.4) and parameters $\theta(P) = 0$, $k(P) = 3.2 - \frac{3.1P}{0.6+P}$, $\alpha = 15.5$, $\nu \in [0, 10]$, and $\beta = 0.97$. We see that increasing ν, the rate of natural death, the solution goes through period doubling bifurcation for $\nu \approx 0.2$ and shrinks the oscillation of the periodic solution; the solution becomes chaotic around $\nu \approx 2$, continuing to increase ν causes the oscillations to decrease; when $\nu \approx 7.5$ the dynamics change to essential extinction (Figure 2.6 (a)). In Figure 2.6 (b), we see that for $\nu \in [0, \psi]$, $\psi \approx 5.5$, the ony positive solution is the carrying capacity; with $\nu \approx 5.5$, an Allee threshold comes into existence. As ν is increased, the carrying capacity decreases and the Allee threshold increases (after it comes into existence). If we let $\nu = 8$, we see that model (2.1) has the strong Allee effect and a growth function with overcompensation and a cusp (Figure 2.6 (c)).

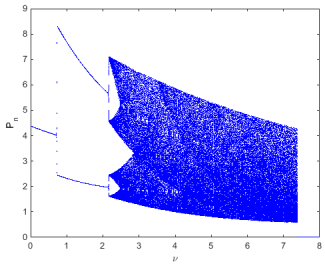

(a) Attracting Solutions for model (2.1) with $\nu \in [0, 8]$ and $P_0 = 1.5$

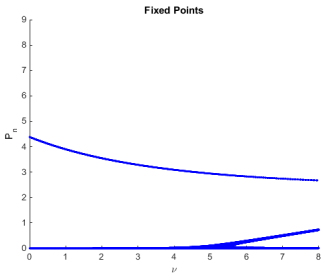

(b) Fixed Points for model (2.1) with $\nu \in [0, 8]$

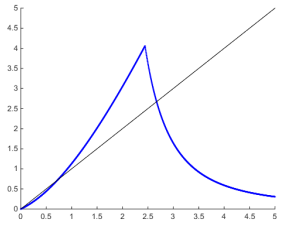

(c) Numerical Approximation of the Growth Function for model (2.1) with $\nu = 8$

$\theta(P) = 0.1$, $k(P) = 3.2 - \frac{3.1P}{1+P}$, $\alpha = 15$, $\nu \in [0, 8]$, $\beta = 0.5$

Figure 2.7: Bifurcation and Fixed Point Diagrams for $\nu \in [0, 8]$ and Growth Function for $\nu = 8$ with $g(P, t)$ given by Equation (2.4)

Consider model (2.1) with the phenology function, $g(P, t)$, as defined in equation (2.4) and parameters $\theta(P) = 0.1$, $k(P) = 3.2 - \frac{3.1P}{1+P}$, $\alpha = 15$, $\nu \in [0, 8]$, and $\beta = 0.5$. We see that increasing ν (the rate of natural death) the solution goes through period doubling bifurcation for $\nu \approx 0.7$ and shrinks the oscillation of the periodic solution; the solution becomes chaotic for $\nu \approx 2.1$ and continuing to increase ν causes the oscillations to decrease; when $\nu \approx 7.4$ the dynamics change to essential extinction (Figure 2.7 (a)). In Figure 2.7 (b) we see that for $\nu \in [0, \psi]$, $\psi \approx 5.4$, the only positive solution is the carrying capacity, with $\nu \approx 5.4$ an Allee threshold comes into existence. As ν is increased, the carrying capacity decreases and the Allee threshold increases (after it comes into existence). If we let $\nu = 8$, we see that model (2.1) has the strong Allee effect and a growth function with overcompensation and a cusp (Figure 2.7 (c)).

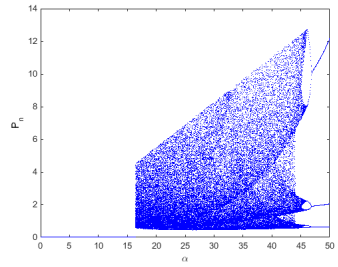

(a) Attracting Solutions for model (2.1) with $\alpha \in [0, 50]$ and $P_0 = 1.5$

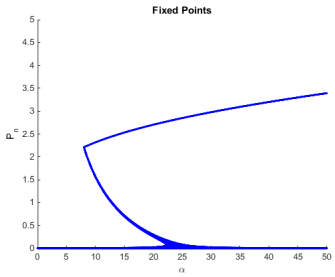

(b) Fixed Points for model (2.1) with $\alpha \in [0, 50]$

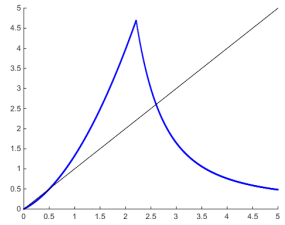

(c) Numerical Approximation of the Growth Function for model (2.1) with $\alpha = 17$

$\theta(P) = 0$, $k(P) = 3.2 - \frac{3.195P}{1+P}$, $\alpha \in [0, 50]$, $\nu = 8$, $\beta = 0.0001$

Figure 2.8: Bifurcation and Fixed Point Diagrams for $\alpha \in [0, 50]$ and Growth Function for $\alpha = 17$ with $g(P, t)$ given by Equation (2.4)

Consider model (2.1) with the phenology function, $g(P, t)$, as defined in equation (2.4) and parameters $\theta(P) = 0$, $k(P) = 3.2 - \frac{3.195P}{1+P}$, $\alpha \in [0, 50]$, $\nu = 8$, and $\beta = 0.0001$. We see that increasing α (the average number of offspring per adult that survive the winter season) causes the existence of a positive carrying capacity and an Allee threshold to come into existence for $\alpha \approx 8$ (for $\alpha \in [0, \psi]$, $\psi \approx 8$, the trivial solution is the only solution for model (2.1)). As α increases, the carrying capacity increases and the Allee threshold decreases (until $\alpha \approx 24.5$ when the Allee threshold disappears) (Figure 2.8 (b)). In Figure 2.8 (a) we see that for $\alpha \in [0, \psi]$, $\psi \approx 16$, the only stable solution is the trivial solution. When $\alpha \approx 16$, the dynamics change to chaos and the magnitude of oscillations increase as α is increased; when $\alpha \approx 46$ the dynamics change to periodic solutions and undergoes period halfing for $\alpha \approx 47$ (Figure 2.8 (a)). If we let $\alpha = 17$, we see that model (2.1) has the strong Allee effect and a growth function with overcompensation and a cusp (Figure 2.8 (c)).

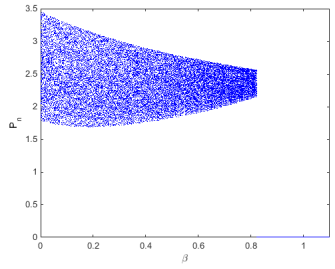

(a) Attracting Solutions for model (2.1) with $\beta \in [0, 1.1]$ and $P_0 = 2.1$

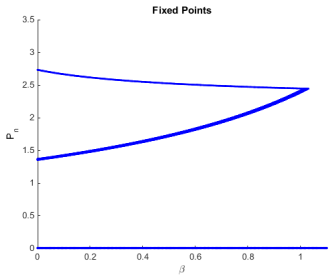

(b) Fixed Points for model (2.1) with $\beta \in [0, 1.1]$

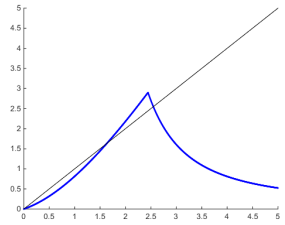

(c) Numerical Approximation of the Growth Function for model (2.1) with $\beta = 0.4$

$\theta(P) = 0$, $k(P) = 3.2 - \frac{3.1P}{1+P}$, $\alpha = 8.5$, $\nu = 6$, $\beta \in [0, 1.1]$

Figure 2.9: Bifurcation and Fixed Point Diagrams for $\beta \in [0, 1.1]$ and Growth Function for $\beta = 0.4$ with $g(P, t)$ given by Equation (2.4)

Consider model (2.1) with the phenology function, $g(P, t)$, as defined in equation (2.4) and parameters $\theta(P) = 0$, $k(P) = 3.2 - \frac{3.1P}{1+P}$, $\alpha = 8.5$, $\nu = 6$, and $\beta \in [0, 1.1]$. We see that increasing β, the rate of competition between adults, decreases the carrying capacity while simultaneously increasing the Allee threshold (Figure 2.9 (b)); when $\beta \approx 1.05$ the carrying capacity and Allee threshold intersect and disappear leaving the trivial solution as the only solution to model (2.1). In Figure 2.9 (a) we see that the model starts out with chaotic dynamics and increasing β decreases the magnitude of oscillation; with $\beta \approx 0.805$ the population drops below the Allee threshold and dies out. If we let $\beta = 0.4$, we see that model (2.1) has the strong Allee effect and a growth function with overcompensation and a cusp (Figure 2.9 (c)).

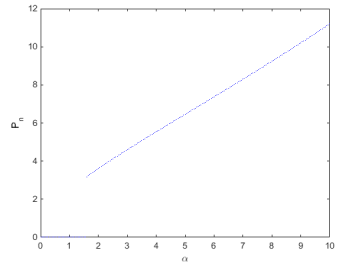

(a) Attracting Solutions for model (2.1) with $\alpha \in [0, 10]$ and $P_0 = 2$

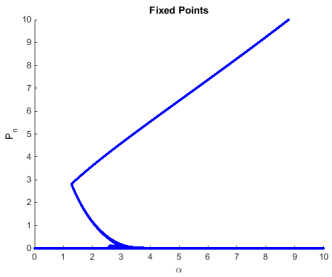

(b) Fixed Points for model (2.1) with $\alpha \in [0, 10]$

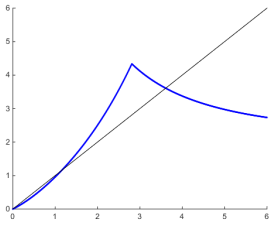

(c) Numerical Approximation of the Growth Function for model (2.1) with $\alpha = 2$

$\theta(P) = \frac{0.9P}{1+P}$, $k(P) = 0.2 + \frac{4.5P}{13+P}$, $\alpha \in [0, 10]$, $\nu = 1.3$, $\beta = 0.1$

Figure 2.10: Bifurcation and Fixed Point Diagrams for $\alpha \in [0, 10]$ and Growth Function for $\alpha = 2$ with $g(P, t)$ given by Equation (2.4)

Consider model (2.1) with the phenology function, $g(P, t)$, as defined in equation (2.4) and parameters $\theta(P) = \frac{0.9P}{1+P}$, $k(P) = 0.2 + \frac{4.5P}{13+P}$, $\alpha \in [0, 10]$, $\nu = 1.3$, and $\beta = 0.1$. We see that with $\alpha \in [0, \psi]$, with $\psi \approx 1.6$, the only equilibrium is the trivail solution (Figure 2.10 (a)). As we increase α (the average number of offspring per adult that survive the winter season) a positive equilibrium and Allee threshold come into existence when $\alpha \approx 1.6$ (Figure 2.10 (b)); as α increases, the carrying capacity increases and the Allee threshold simultaneously decreases until $\alpha \approx 3.1$ when the Allee threshold disappears. If we let $\alpha = 2$, we see that model (2.1) has the strong Allee effect and a growth function with overcompensation and a cusp (Figure 2.10 (c)).

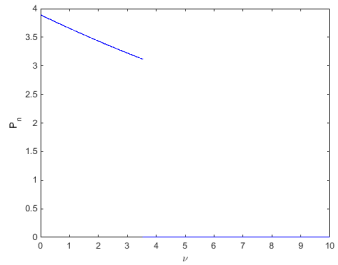

(a) Attracting Solutions for model (2.1) with $\nu \in [0, 10]$ and $P_0 = 2.5$

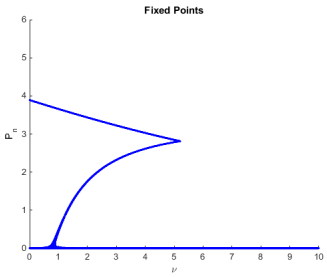

(b) Fixed Points for model (2.1) with $\nu \in [0, 10]$

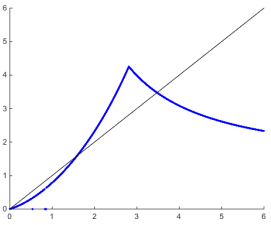

(c) Numerical Approximation of the Growth Function for model (2.1) with $\nu = 1.8$

$\theta(P) = \frac{0.95P}{1+P}$, $k(P) = 0.2 + \frac{4.5P}{13+P}$, $\alpha = 2$, $\nu = 1.8$, $\beta = 0.05$

Figure 2.11: Bifurcation and Fixed Point Diagrams for $\nu \in [0, 10]$ and Growth Function for $\nu = 1.8$ with $g(P, t)$ given by Equation (2.4)

Consider model (2.1) with the phenology function, $g(P, t)$, as defined in equation (2.4) and parameters $\theta(P) = \frac{0.95P}{1+P}$, $k(P) = 0.2 + \frac{4.5P}{13+P}$, $\alpha = 2$, $\nu = 1.8$, and $\beta = 0.05$. We see that increasing ν (the rate of natural death) decreases the carrying capacity until $\nu \approx 3.6$ when the model enters essential extinction (Figure 2.11 (a)); increasing ν aslo casues an Allee threshold to come into existence when $\nu \approx 0.8$, the Allee threshold increases (as ν is increased) until it intersects the carrying capacity, $\nu \approx 5.2$, at which point the carrying capacity and the Allee threshold disappear (Figure 2.11 (b)). If we let $\nu = 1.8$, we see that model (2.1) has the strong Allee effect and a growth function with overcompensation and a cusp (Figure 2.11 (c)).

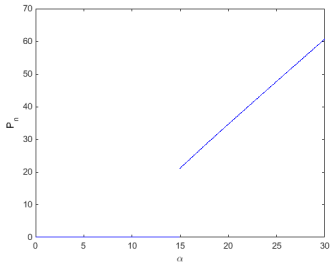

(a) Attracting Solutions for model (2.1) with $\alpha \in [0, 30]$ and $P_0 = 2$

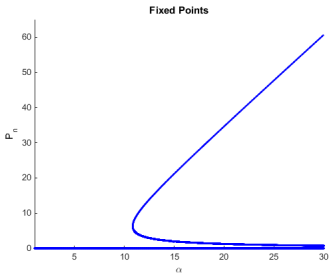

(b) Fixed Points for model (2.1) with $\alpha \in [0, 30]$

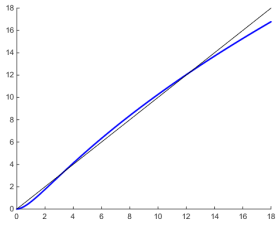

(c) Numerical Approximation of the Growth Function for model (2.1) with $\alpha = 12$

$\theta(P) = \frac{0.5P}{0.5+P}$, $k(P) = 0.5 + \frac{0.5P}{0.8+P}$, $\alpha \in [0, 30]$, $\nu = 6.5$, $\beta = 0.5$

Figure 2.12: Bifurcation and Fixed Point Diagrams for $\alpha \in [0, 30]$ and Growth Function for $\alpha = 12$ with $g(P, t)$ given by Equation (2.4)

Consider model (2.1) with the phenology function, $g(P, t)$, as defined in equation (2.4) and parameters $\theta(P) = \frac{0.5P}{0.5+P}$, $k(P) = 0.5 + \frac{0.5P}{0.8+P}$, $\alpha \in [0, 30]$, $\nu = 6.5$, and $\beta = 0.5$. We see that for α (the average number of offspring per adult that survive the winter season) between 0 and approximately 14.95, that the trivial solution is the only stable equilibrium and when $\alpha \approx 14.95$ a stable positive equilibrium comes into existence ant the equilibrium increases as α increases (Figure 2.12 (a)). For α between 0 and approximately 11.1, the only equilibrium point is the trivial solution. When $\alpha \approx 11.1$, an Allee threshold and carrying capacity come into existence; as α increases, the carrying capacity increases and the Allee threshold decreases (Figure 2.12 (b)). If we let $\alpha = 12$, we see that model (2.1) has the strong Allee effect and a monotone growth function (Figure 2.12 (c)).

2.2.2 WHEN THE PHENOLOGY FUNCTION IS THE GAMMA DISTRIBUTION

Consider the gamma distribution given by:

$$g(P,t) = \frac{t^{k(P)-1}e^{-t/\theta(P)}}{\Gamma(k(P))\theta^{k(P)}} \tag{2.7}$$

Where $k(P)$ is the shape parameter, $\theta(P)$ is the scale parameter, and $\Gamma(k)$ is the gamma function. How these parameters affect the gamma distribution can be seen in Figure 2.13.

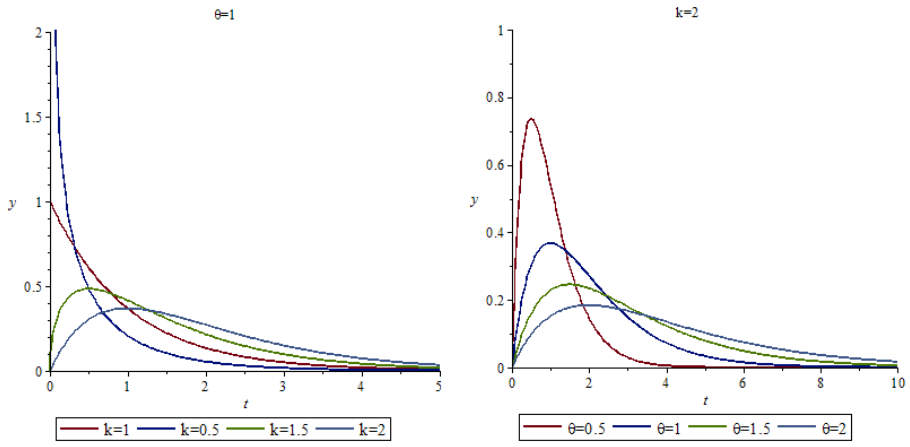

(a) $g(P,t)$ for different values of k with θ fixed

(b) $g(P,t)$ for different values of θ with k fixed

Figure 2.13: How the parameters affect the gamma distribution

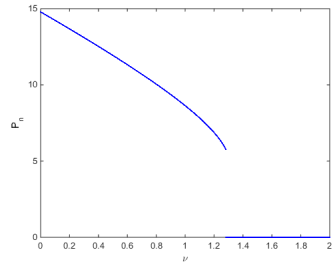

(a) Attracting Solutions for model (2.1) with $\nu \in [0, 2]$ and $P_0 = 4$

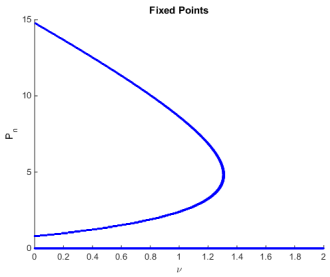

(b) Fixed Points for model (2.1) with $\nu \in [0, 2]$

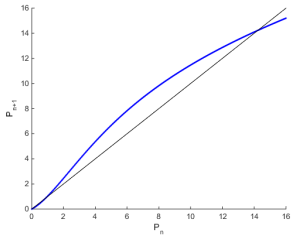

(c) Numerical Approximation of the Growth Function for model (2.1) with $\nu = 0.1$

$\theta(P) = 0.5$, $k(P) = 4 - \frac{2P}{3+P}$, $\alpha = 5$, $\nu \in [0, 2]$, $\beta = 0.2$

Figure 2.14: Bifurcation and Fixed Point Diagrams for $\nu \in [0, 2]$ and Growth Function for $\nu = 0.1$ with $g(P, t)$ given by Equation (2.7)

Consider model (2.1) with the phenology function, $g(P, t)$, as defined in equation (2.7) and parameters $\theta(P) = 0.5$, $k(P) = 4 - \frac{2P}{3+P}$, $\alpha = 5$, $\nu \in [0, 2]$, and $\beta = 0.2$. We see that increasing ν (the rate of natural death) decreases the carrying capacity while simultaneously increasing the Allee threshold (Figure 2.14 (b)); with $\nu \approx 1.31$ the carrying capacity and Allee threshold intersect and then disappear, leaving the trivial solution as the only solution to model (2.1). In Figure 2.14 (a) we see that the model starts off with a stable period one solution that decreases as ν is increases; when $\nu \approx 1.29$, the population drops below the Allee threshold and becomes extinct (for ν larger than ≈ 1.31 the trivial solution is the only solution). If we let $\nu = 0.1$, we see that model (2.1) the strong Allee effect and a monotone growth function (Figure 2.14 (c)).

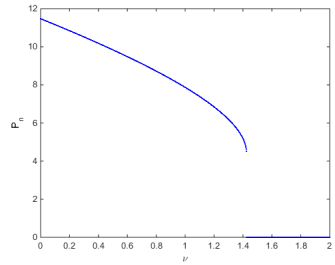

(a) Attracting Solutions for model (2.1) with $\nu \in [0, 2]$ and $P_0 = 5$

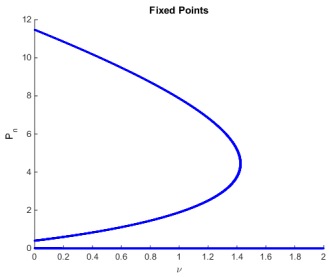

(b) Fixed Points for model (2.1) with $\nu \in [0, 2]$

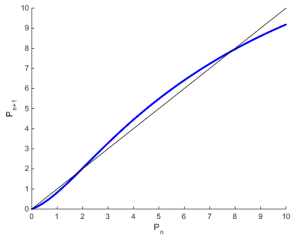

(c) Numerical Approximation of the Growth Function for model (2.1) with $\nu = 1$

$\theta(P) = 10 - \frac{9.95P}{1+P}$, $k(P) = 1$, $\alpha = 8$, $\nu \in [0, 2]$, $\beta = 0.3$

Figure 2.15: Bifurcation and Fixed Point Diagrams for $\nu \in [0, 2]$ and Growth Function for $\nu = 1$ with $g(P, t)$ given by Equation (2.7)

Consider model (2.1) with the phenology function, $g(P, t)$, as defined in equation (2.7) and parameters $\theta(P) = 10 - \frac{9.95P}{1+P}$, $k(P) = 1$, $\alpha = 8$, $\nu \in [0, 2]$, and $\beta = 0.3$. We see that increasing ν (the rate of natural death) causes the carrying capacity to decrease (Figure 2.15 (a)) while simultaneously causing the Allee threshold to increase. When $\nu \approx 1.41$, the Allee threshold and carrying capacity intersect and disappear, leaving the trivial solution as the only equilibrium (Figure 2.15 (b)). If we let $\nu = 1$, we see that model (2.1) has the strong Allee effect and a monotone growth function (Figure 2.15 (c)).

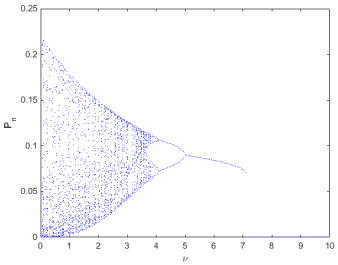

(a) Attracting Solutions for model (2.1) with $\nu \in [0, 10]$ and $P_0 = 0.08$

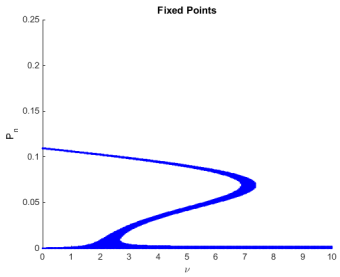

(b) Fixed Points for model (2.1) with $\nu \in [0, 10]$

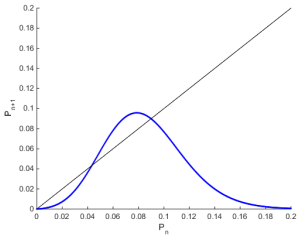

(c) Numerical Approximation of the Growth Function for model (2.1) with $\nu = 5$

$\theta(P) = 0.1$, $k(P) = 1.1 + \frac{125P}{1+P}$, $\alpha = 6$, $\nu \in [0, 10]$, $\beta = 5$

Figure 2.16: Bifurcation and Fixed Point Diagrams for $\nu \in [0, 10]$ and Growth Function for $\nu = 5$ with $g(P, t)$ given by Equation (2.7)

Consider model (2.1) with the phenology function, $g(P, t)$, as defined in equation (2.7) and parameters $\theta(P) = 0.1$, $k(P) = 1.1 + \frac{125P}{1+P}$, $\alpha = 6$, $\nu \in [0, 10]$, and $\beta = 5$. In Figure 2.16 (a), we see that the model starts with chaotic dynamics and increasing ν (the rate of natural death) the magnitude of oscillations decrease; when $\nu \approx 3.99$, the dynamics change to periodic solutions and goes through period undoubling for $\nu \approx 4.05$ and $\nu \approx 5$; for ν larger than ≈ 7.1 the only solution is the trivial solution. In Figure 2.16 (b), we see that the model starts with only one positive equilibrium (the carrying capacity) and gains a second positive equilibrium (the Allee threshold) for $\nu \approx 2.5$. As ν is increased, the carrying capacity decreases and the Allee threshold increases (after it comes into existence); with $\nu \approx 7.1$ the carrying capacity and Allee threshold intersect and then disappear, leaving the trivial solution as the only equilibrium solution. If we let $\nu = 5$, we see that model (2.1) has the strong Allee effect and a smooth growth function with overcompensation (Figure 2.16 (c)).

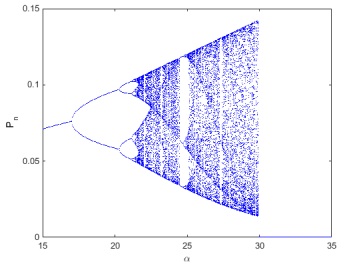

(a) Attracting Solutions for model (2.1) with $\alpha \in [0, 35]$ and $P_0 = 0.06$

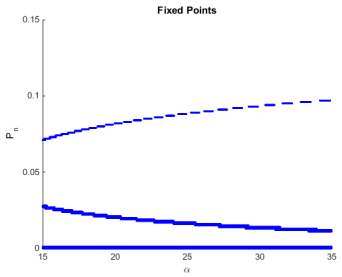

(b) Fixed Points for model (2.1) with $\alpha \in [0, 35]$

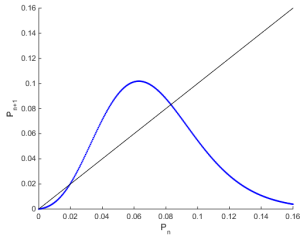

(c) Numerical Approximation of the Growth Function for model (2.1) with $\alpha = 21$

$\theta(P) = 0.2$, $k(P) = 1.1 + \frac{85P}{1+P}$, $\alpha = 21$, $\nu = 10$, $\beta = 6$

Figure 2.17: Bifurcation and Fixed Point Diagrams for $\alpha \in [0, 35]$ and Growth Function for $\alpha = 21$ with $g(P, t)$ given by Equation (2.7)

Consider model (2.1) with the phenology function, $g(P, t)$, as defined in equation (2.7) and parameters $\theta(P) = 0.2$, $k(P) = 1.1 + \frac{85P}{1+P}$, $\alpha = 21$, $\nu = 10$, and $\beta = 6$. In Figure 2.17 (b) we see that increasing α, the average number of offspring per adult that survive the winter, increases the carrying capacity while simultaneously decreasing the Allee threshold. In Figure 2.17 (a) the model has a stable attractor (which increases while α increases) for $\alpha \in [15], \psi$, $\psi \approx 17$; the model goes through period doubling bifurcation for $\alpha \approx 17$ and $\alpha \approx 20.1$, with the magnitude of oscillations increasing as α increases; the model changes to chaotic dynamics when $\alpha \approx 21$, with the oscillations increasing as α increases; when α is greater than ≈ 30, the only stable solution is the trivial solution. If we let $\alpha = 21$, we see that model (2.1) has the strong Allee effect and a smooth growth function with overcompensation (Figure 2.17 (c)).

2.2.3 WHEN THE PHENOLOGY FUNCTION IS THE GENERALIZED BETA DISTRIBUTION

Consider the generalized beta distribution given by:

$$g(P,t) = \begin{cases} h(P,t) & \text{,if } 0 \leq t^{a1} \leq \dfrac{b1^{a1}}{1-k(P)} \\ 0 & \text{, otherwise} \end{cases} \tag{2.8}$$

Where $h(P,t) = \frac{\Gamma(p1+\theta)|a1|t^{a1p1-1}(1-(1-k(P)(\frac{t}{b1})^{a1}))^{\theta-1}}{\Gamma(p1)\Gamma(\theta)(1+k(P)(\frac{t}{b1})^{a1})^{p1+\theta}}$

Where $0 < k(P) < 1$ and $b1, p1, \theta > 0$, and $\Gamma(k)$ is the gamma function. The generalized beta distribution reduces to the beta distribution if $a1 = 1$, i.e.,

$$h(P,t) = \frac{\Gamma(p1+\theta)\ t^{p1-1}(1-(1-k(P))(\frac{t}{b1}))^{\theta-1}}{\Gamma(p1)\Gamma(\theta)(1+k(P)(\frac{t}{b1}))^{p1+\theta}}$$

where $p1$ and θ are shape parameters and $\frac{b1}{1-k(P)}$ is the upper bound of the support. How these parameters affect the generalized beta distribution can be seen in Figure 2.18.

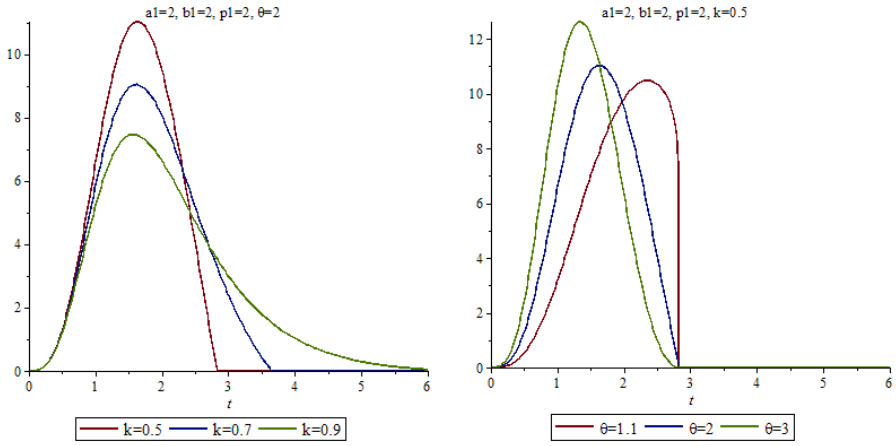

(a) $g(P,t)$ for different values of k (b) $g(P,t)$ for different values of θ

Figure 2.18: How the parameters affect the generalized beta distribution

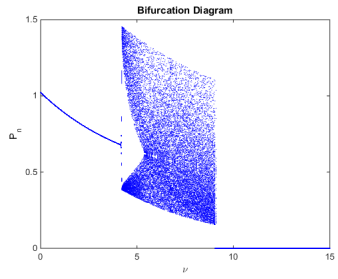

(a) Attracting Solutions for model (2.1) with $\nu \in [0, 15]$ and $P_0 = 0.3$

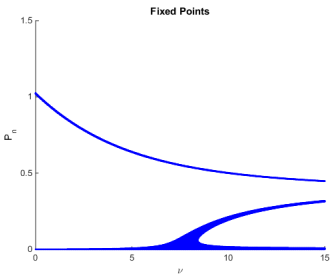

(b) Fixed points for model (2.1) with $\nu \in [0, 15]$

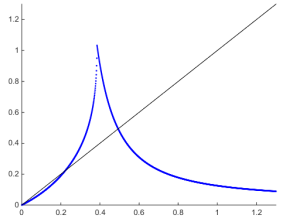

(c) Numerical Approximation of the Growth Function for model (2.1) with $\nu = 10.5$

$\theta(P) = 0.5$, $k(P) = 1 - \frac{0.9P}{1+P}$, $a1 = 2$, $b1 = 0.5$, $p1 = 0.5$, $\alpha = 22$, $\nu \in [0, 15]$, $\beta = 3$

Figure 2.19: Bifurcation and Fixed Point Diagrams for $\nu \in [0, 15]$ and Growth Function for $\nu = 10.5$ with $g(P,t)$ given by Equation (2.8)

Consider model (2.1) with the phenology function, $g(P,t)$, as defined in equation (2.8) and parameters $\theta(P) = 0.5$, $k(P) = 1 - \frac{0.9P}{1+P}$, $a1 = 2$, $b1 = 0.5$, $p1 = 0.5$, $\alpha = 22$, $\nu \in [0, 15]$, and $\beta = 3$. In Figure 2.19 (a), we see that the model starts with a stable period one equilibrium which decreases in magnitude as ν (the rate of nat-

ural death) is increased; with $\nu \approx 4.5$ the dynamics change to chaos, the magnitude of oscillations decrease as ν is increased; for ν larger than ≈ 9, the dynamics change to essential extinction. In Figure 2.19 (b), we see that the model starts with only one positive equilibrium, which is the carrying capacity, and the carrying capacity decreases as ν is increased. When $\nu \approx 7.8$ an Allee threshold comes into existence and increases as ν is increased. If we let $\nu = 10.5$, we see that moel (2.1) has the strong Allee effect and a growth function with overcompensation and a cusp (Figure 2.19 (c)).

CHAPTER 3
THE SPATIAL MODEL

3.1 THE MODEL

Recall the biological assumptions for model (2.1). That is, the within season adult density is denoted by $A(P,t)$ for $t \in [0,1]$ and P_n denotes the initial density of eggs (or seeds) at the begining of the n^{th} year. We consider a population that suffers from natural death at a rate ν and assume that competition between adults is quadratic with coefficient β. The emergence of adults is controlled by phenology, which is density dependent. The phenology kernel is denoted by $g(P,t)$. At the end of the season, adults give birth to eggs (or produce seeds) and then die and any juveniles that have not emmerged into adults by this time also die. The average number of offspring per adult that survive the winter is α. The season ends at time $t = 1$ after the adults have given birth. If we add the assumption that the adults move according to random diffusion processes with diffusion coefficient $D > 0$, during the winter there is no dispersal, and that juveniles are immobile (e.g., eggs or seeds), then the population dynamics are governed by

$$\begin{aligned} &A_t = DA_{xx} + \alpha g(P_n,t)P_n - \nu A - \beta A^2, \quad A(P_n,x,0) = 0 \\ &P_{n+1}(x) = A(P_n,x,1). \end{aligned} \tag{3.1}$$

We make the following assumption on model (3.1) and provide a theorem on the existence of solutions to model (3.1).

HYPOTHESES 3.1.

$g(P,t)$ is a probability density function on $[0,\infty)$.

THEOREM 3.1. *Assume that Hypotheses 3.1 is satisfied. Then model* (3.1) *has a unique positive solution.*

The proof for Theorem 3.1 is a direct application of Theorem 2.2 in chapter 7 of (Pao) and is therefore omitted.

If the phenology function in model (2.1) is only depended on time (i.e., it is not density dependent), then model (3.1) becomes model (3.2), which is a special case of model (1) in Otto et al. (2018). In this case, Otto et al. have shown the existence of traveling wave solutions and calculated the spreading speed for the model.

$$\begin{aligned} &A_t = DA_{xx} + \alpha g(t) P_n - \nu A - \beta A^2, \quad A(x,0) = 0 \\ &P_{n+1}(x) = A(x,1). \end{aligned} \tag{3.2}$$

HYPOTHESES 3.2. *(Otto et al., 2018)*

$g(t)$ is either a piecewise continuous bounded probability density function on $[0,\infty)$ or a Dirac delta function $\delta(t - t_{emg})$ with $t_{emg} > 0$.

For model (3.2), Otto et al. defined the moment-generating function, which is used in calculating the spreading speed.

$$\Lambda(\mu) = L[e^{-\mu x}](0), \tag{3.3}$$

where L is the solution operator of the linearization of model (3.2). Then,

$$c^* = \inf_{\mu>0} \frac{\ln[\Lambda(\mu)]}{\mu} \tag{3.4}$$

where

$$\Lambda(\mu) = \alpha \int_0^1 g(s) e^{(\mu^2 D - \nu)(1-s)} ds \tag{3.5}$$

(see the Appendix for details on L and $\Lambda(\mu)$)

Otto et al. provided the following theorem regarding the spreading speed and traveling wave solutions for model (3.2).

THEOREM 3.2. *(Otto et al., 2018) Assume that Hypotheses 3.2 are satisfied. Let* $\Lambda(0) > 1$. *Then, the following statements are valid for model* (3.2)*:*

1. *There exists a positive constant equilibrium* $P^* > 0$.

2. c^* *is the spreading speed in the following sense:*

   If the continuous initial function $P_0(x)$ *is zero for all sufficiently large* $|x|$, $P_0(x) \not\equiv 0$, *and* $0 \leq P_0(x) \leq P^*$, *then for any small positive* ε, *the solution* $P_n(x)$ *has the following properties*

   (a)
   $$\lim_{n\to\infty} \left[\sup_{|x|\geq n(c^*+\varepsilon)} P_n(x) \right] = 0.$$

   (b)
   $$\lim_{n\to\infty} \left[\sup_{|x|\leq n(c^*-\varepsilon)} |P^* - P_n(x)| \right] = 0.$$

3. *There exists a nonincreasing wave* $P_n(x) = w(x - nc)$ *with* $w(-\infty) = P^*$ *and* $w(-\infty) = 0$ *if and only if* $c \geq c^*$.

The proof of Theorem 3.2 can be found in Otto et al. (2018).

The density dependent phenology makes things very complicated. In the next section we provide numerical simulations to explore the dpatial dynamics.

3.2 NUMERICAL SIMULATIONS FOR MODEL (3.1)

In this section we will explore some to the complex dynamics of model (3.1) through numerical simulations when the phenological functions are the uniform distribution (see Equation (2.4)), gamma distribution (see Equation (2.7)), and the generalized beta distribution (see Equation (2.8)). When discussing solutions to our spatial model, we call a nonnegative solution (that is not identically zero) that spreads in both directions a wave solution. If the wave solution oscillates, and the oscillations appear to follow a pattern, it is called an oscillating wave solution. If the wave solution oscillates, and the oscillations do not appear to follow a pattern, it is called a chaotic wave solution.

We show that model (3.1) can exhibit wave solutions (Figures 3.1 (a), 3.10 (a), 3.12 (a), 3.13 (a), and 3.14 (a)), oscillating wave solutions (Figures 3.2 (a), 3.3 (a), and 3.4 (a)), chaotic wave solutions (Figures 3.5 (a), 3.6 (a), 3.7 (a), 3.8 (a), 3.17 (a), and 3.18 (a)) and nonspreading solutions (Figures 3.9 (a), 3.11 (a), 3.15 (a), and 3.16 (a)). It is also shown that the solutions of model (3.1) can have constant (Figures 3.1 (b), 3.2 (b), 3.3 (b), 3.4 (b), 3.12 (b), 3.13 (b), and 3.14 (b)), oscillating (Figures 3.5 (b), 3.6 (b), 3.7 (b), 3.8 (b), and 3.10 (b)), and chaotic (Figures 3.17 (b) and 3.18 (b)) spreading speed.

As in Section 2.2, we assume that the density-dependent parameters of the phenological function are either nonincreasing or nondecreasing. All of the numerical simulations for model (3.1) we done in Mathematica. To create the figures showing the year-to-year population distribution, the built-in function NDSolve

was used. To numerically calculate the spreading speed, we define a level set, L, and then minimize the solutions of $(P_n(x) - L)^2$; then we take the difference of consecutive solutions of the minimization.

We use the indicator function

$$\chi_A(x) = \begin{cases} 1 & x \in A \\ 0 & x \notin A \end{cases}$$

to help define the initial distribution $P_0(x)$.

3.2.1 WHEN THE PHENOLOGY FUNCTION IS THE UNIFORM DISTRIBUTION

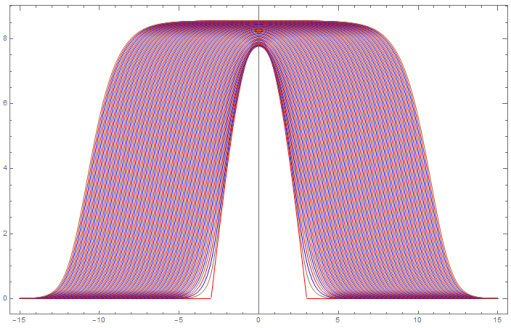

(a) Solutions $P_0(x)$ through $P_{100}(x)$ for model (3.1)

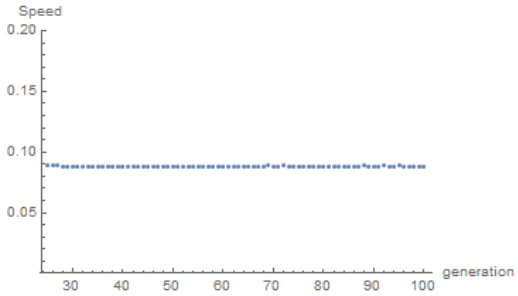

(b) Spreading speed for model (3.1)

$D = 1$, $\theta(P) = 0$, $k(P) = 3.2 - \frac{2.25P}{0.4+P}$, $\alpha = 9$, $\nu = 6$, $\beta = 0.3$, $P_0(x) = 8\cos(\frac{\pi x}{6})\chi_{[-3,3]}(x)$, $L = 1$.

Figure 3.1: Wave Solutions with Constant Spreading Speed for Model (3.1) with $g(P,t)$ given by Equation (2.4)

Consider the phenology function, $g(P,t)$, as defined in equation (2.4) and parameters $D = 1$, $\theta(P) = 0$, $k(P) = 3.2 - \frac{2.25P}{0.4+P}$, $\alpha = 9$, $\nu = 6$, $\beta = 0.3$, and $P_0(x) = 8\cos(\frac{\pi x}{6})\chi_{[-3,3]}(x)$. We see that model (3.1) has wave solutions (Figure 3.1

(a)) which grow from $P_0(x)$ to the carrying capacity and spreads in both directions with constant spreading speed (Figure 3.1 (b)).

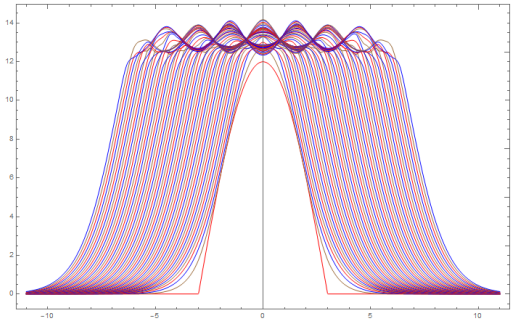

(a) Solutions $P_0(x)$ through $P_{100}(x)$ for model (3.1)

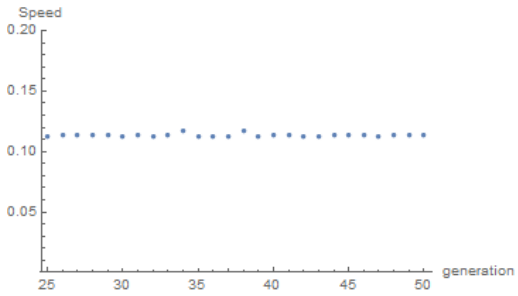

(b) Spreading speed for model (3.1)

$D = 1$, $\theta(P) = 0$, $k(P) = 3.2 - \frac{3.1P}{5+P}$, $\alpha = 3.4$, $\nu = 1.5$, $\beta = 0.1$, $P_0(x) = 12\cos(\frac{\pi x}{6})\chi_{[-3,3]}(x)$, $L = 1$.

Figure 3.2: Oscillating Wave Solutions with Constant Spreading Speed for Model (3.1) with $g(P,t)$ given by Equation (2.4)

Consider the phenology function, $g(P,t)$, as defined in equation (2.4) and parameters $D = 1$, $\theta(P) = 0$, $k(P) = 3.2 - \frac{3.1P}{5+P}$, $\alpha = 3.4$, $\nu = 1.5$, $\beta = 0.1$, and $P_0(x) = 12\cos(\frac{\pi x}{6})\chi_{[-3,3]}(x)$. We see that solutions of model (3.1) grow from $P_0(x)$ to wave solutions that oscillate around the carrying capacity (Figure 3.2 (b)) and spreads in both directions with constant spreading speed (Figure 3.2 (a)).

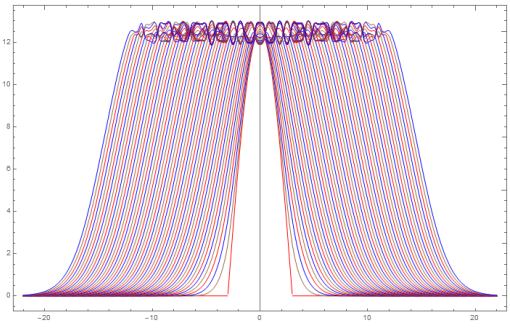

(a) Solutions $P_0(x)$ through $P_{50}(x)$ for model (3.1)

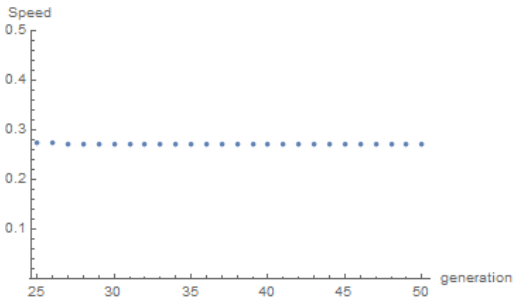

(b) Spreading speed for model (3.1)

$D = 1$, $\theta(P) = 0$, $k(P) = 3.2 - \frac{3.1P}{5+P}$, $\alpha = 3.3$, $\nu = 0.4$, $\beta = 0.21$, $P_0(x) = 12.5\cos(\frac{\pi x}{6})\chi_{[-3,3]}(x)$, $L = 1$.

Figure 3.3: Oscillating Wave Solutions with Constant Spreading Speed for Model (3.1) with $g(P,t)$ given by Equation (2.4)

Consider the phenology function, $g(P,t)$, as defined in equation (2.4) and parameters $D = 1$, $\theta(P) = 0$, $k(P) = 3.2 - \frac{3.1P}{5+P}$, $\alpha = 3.3$, $\nu = 0.4$, $\beta = 0.21$, and $P_0(x) = 12.5\cos(\frac{\pi x}{6})\chi_{[-3,3]}(x)$. We see that solutions of model (3.1) grow from $P_0(x)$ to wave solutions that oscillate around the carrying capacity (Figure 3.3 (a)) and spreads in both directions with a constant spreading speed (Figure 3.3 (b)).

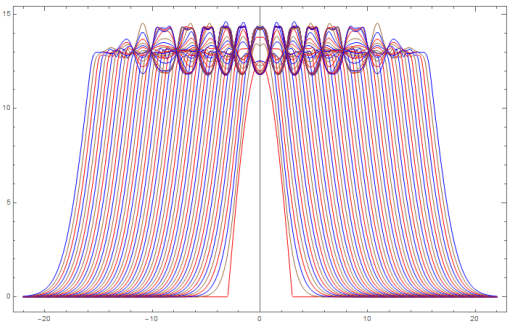

(a) Solutions $P_0(x)$ through $P_{50}(x)$ for model (3.1)

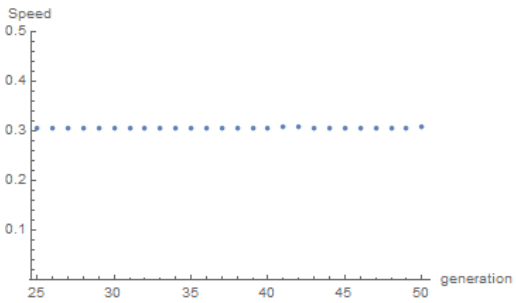

(b) Spreading speed for model (3.1)

$D = 1$, $\theta(P) = 0.18$, $k(P) = 3.2 - \frac{3.1P}{5+P}$, $\alpha = 3.3$, $\nu = 0.4$, $\beta = 0.21$, $P_0(x) = 12.5\cos(\frac{\pi x}{6})\chi_{[-3,3]}(x)$, $L = 1$.

Figure 3.4: Oscillating Wave Solutions with Constant Spreading Speed for Model (3.1) with $g(P,t)$ given by Equation (2.4)

Consider the phenology function, $g(P,t)$, as defined in equation (2.4) and parameters $D = 1$, $\theta(P) = 0.18$, $k(P) = 3.2 - \frac{3.1P}{5+P}$, $\alpha = 3.3$, $\nu = 0.4$, $\beta = 0.21$, and $P_0(x) = 12.5\cos(\frac{\pi x}{6})\chi_{[-3,3]}(x)$. We see that model (3.1) wave solutions (Figure 3.4 (a)) which grow from $P_0(x)$, oscillate around the carrying capacity, and spreads in both directions with a constant spreading speed (Figure 3.4 (b)).

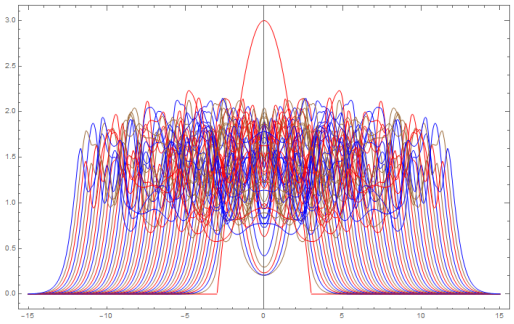

(a) Solutions $P_0(x)$ through $P_{50}(x)$ for model (3.1)

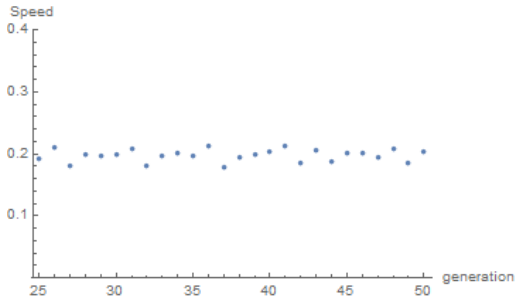

(b) Spreading speed for model (3.1)

$D = 1$, $\theta(P) = 0$, $k(P) = 3.2 - \frac{3.1P}{0.6+P}$, $\alpha = 16$, $\nu = 8$, $\beta = 1$, $P_0(x) = 3\cos(\frac{\pi x}{6})\chi_{[-3,3]}(x)$, $L = 0.25$.

Figure 3.5: Chaotic Wave Solutions with Oscillating Spreading Speed for Model (3.1) with $g(P,t)$ given by Equation (2.4)

Consider the phenology function, $g(P,t)$, as defined in equation (2.4) and parameters $D = 1$, $\theta(P) = 0$, $k(P) = 3.2 - \frac{3.1P}{0.6+P}$, $\alpha = 16$, $\nu = 8$, $\beta = 1$, and $P_0(x) = 3\cos(\frac{\pi x}{6})\chi_{[-3,3]}(x)$. We see that model (3.1) has chaotic wave solutions (Figure 3.5 (a)) which grow from $P_0(x)$ and spreads in both directions with an oscillating spreading speed (Figure 3.5 (b)). The wave solutions for model (3.1) are persistent even though the nonspatial dynamics of model (2.1) is essential extinction.

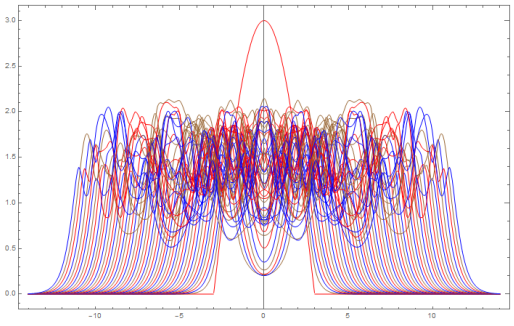

(a) Solutions $P_0(x)$ through $P_{50}(x)$ for model (3.1)

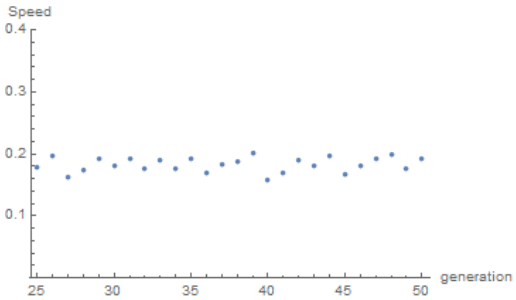

(b) Spreading speed for model (3.1)

$D = 1$, $\theta(P) = 0$, $k(P) = 3.2 - \frac{3.1P}{0.6+P}$, $\alpha = 15.5$, $\nu = 8$, $\beta = 0.97$, $P_0(x) = 3\cos(\frac{\pi x}{6})\chi_{[-3,3]}(x)$, $L = 0.25$.

Figure 3.6: Chaotic Wave Solutions with Oscillating Spreading Speed for Model (3.1) with $g(P,t)$ given by Equation (2.4)

Consider the phenology function, $g(P,t)$, as defined in equation (2.4) and parameters $D = 1$, $\theta(P) = 0$, $k(P) = 3.2 - \frac{3.1P}{0.6+P}$, $\alpha = 15.5$, $\nu = 8$, $\beta = 0.97$, and $P_0(x) = 3\cos(\frac{\pi x}{6})\chi_{[-3,3]}(x)$. We see that model (3.1) has chaotic wave solutions (Figure 3.6 (a)) which grow from $P_0(x)$ and spreads in both directions with an oscillating spreading speed (Figure 3.6 (b)).

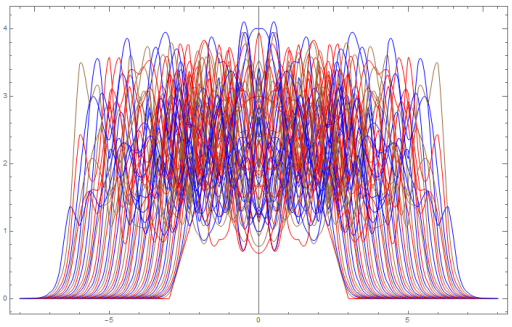

(a) Solutions $P_0(x)$ through $P_{50}(x)$ for model (3.1)

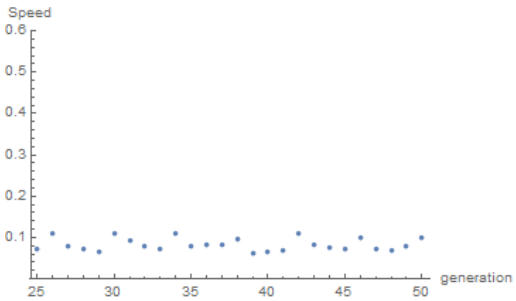

(b) Spreading speed for model (3.1)

$D = 0.2$, $\theta(P) = 0.1$, $k(P) = 3.2 - \frac{3.1P}{1+P}$, $\alpha = 15$, $\nu = 8$, $\beta = 0.5$, $P_0(x) = 3\cos(\frac{\pi x}{6})\chi_{[-3,3]}(x)$, $L = 0.1$.

Figure 3.7: Chaotic Wave Solutions with Oscillating Spreading Speed for Model (3.1) with $g(P,t)$ given by Equation (2.4)

Consider the phenology function, $g(P,t)$, as defined in equation (2.4) and parameters $D = 0.2$, $\theta(P) = 0.1$, $k(P) = 3.2 - \frac{3.1P}{1+P}$, $\alpha = 15$, $\nu = 8$, $\beta = 0.5$, and $P_0(x) = 3\cos(\frac{\pi x}{6})\chi_{[-3,3]}(x)$. We see that model (3.1) has chaotic wave solutions (Figure 3.7 (a)) which grow from $P_0(x)$ and spreads in both directions with an oscillating spreading speed (Figure 3.7 (b)).

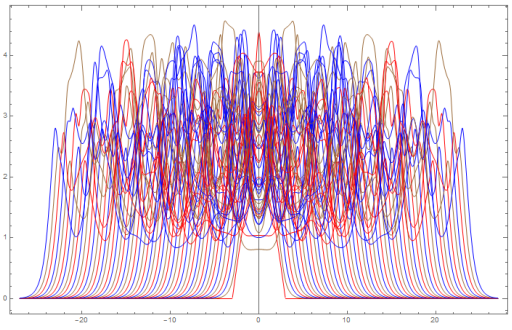

(a) Solutions $P_0(x)$ through $P_{50}(x)$ for model (3.1)

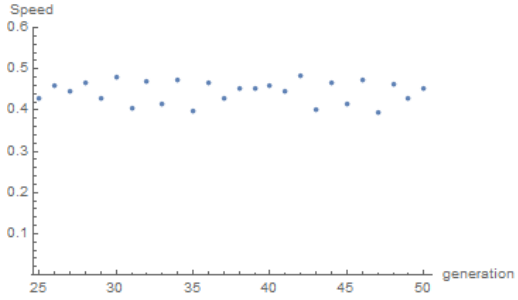

(b) Spreading speed for model (2.1)

$D = 2$, $\theta(P) = 0$, $k(P) = 3.2 - \frac{3.195P}{1+P}$, $\alpha = 17$, $\nu = 8$, $\beta = 0.0001$, $P_0(x) = 2\cos(\frac{\pi x}{6})\chi_{[-3,3]}(x)$, $L = 0.25$

Figure 3.8: Chaotic Wave Solutions with Oscillating Spreading Speed for Model (3.1) with $g(P,t)$ given by Equation (2.4)

Consider the phenology function, $g(P,t)$, as defined in equation (2.4) and parameters $D = 2$, $\theta(P) = 0$, $k(P) = 3.2 - \frac{3.195P}{1+P}$, $\alpha = 17$, $\nu = 8$, $\beta = 0.0001$, and $P_0(x) = 2\cos(\frac{\pi x}{6})\chi_{[-3,3]}(x)$. We see that model (3.1) has chaotic wave solutions (Figure 3.8 (a)) which grow from $P_0(x)$ and spreads in both directions with an oscillating spreading speed (Figure 3.8 (b)).

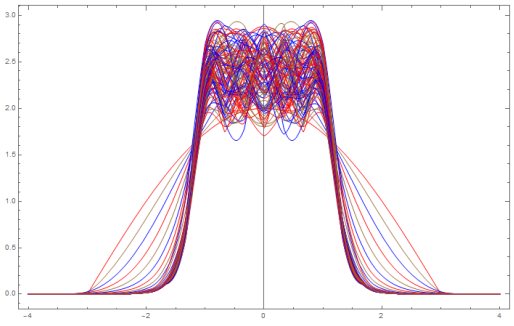

(a) Solutions $P_0(x)$ through $P_{100}(x)$ for model (3.1)

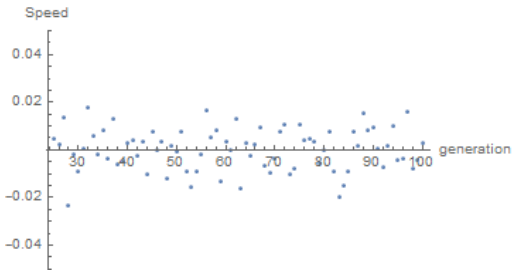

(b) Spreading speed for model (3.1)

$D = 0.1$, $\theta(P) = 0$, $k(P) = 3.2 - \frac{3.1P}{1+P}$, $\alpha = 8.5$, $\nu = 6$, $\beta = 0.4$, $P_0(x) = 2\cos(\frac{\pi x}{6})\chi_{[-3,3]}(x)$, $L = 1$.

Figure 3.9: Nonspreading Solution for Model (3.1) with $g(P,t)$ given by Equation (2.4)

Consider the phenology function, $g(P,t)$, as defined in equation (2.4) and parameters $D = 0.1$, $\theta(P) = 0$, $k(P) = 3.2 - \frac{3.1P}{1+P}$, $\alpha = 8.5$, $\nu = 6$, $\beta = 0.4$, and $P_0(x) = 2\cos(\frac{\pi x}{6})\chi_{[-3,3]}(x)$. We see that solutions of model (3.1) grow from $P_0(x)$ to an unstable nonspreading solution, i.e. the solution oscillates but does not spread in time (Figures 3.9 (a) and (b)).

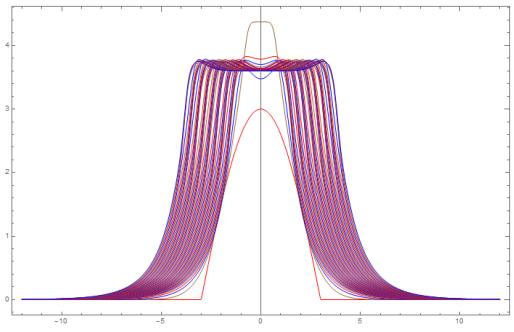

(a) Solutions $P_0(x)$ through $P_{50}(x)$ for model (3.1)

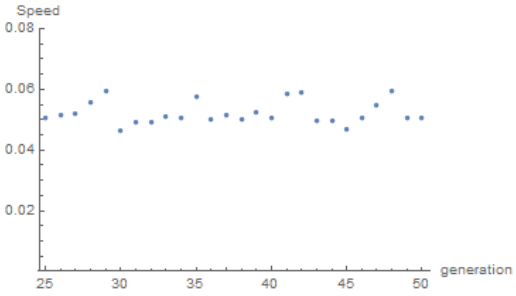

(b) Spreading speed for model (3.1)

$D = 1$, $\theta(P) = \frac{0.9P}{1+P}$, $k(P) = 0.2 + \frac{4.5P}{13+P}$, $\alpha = 2$, $\nu = 1.3$, $\beta = 0.1$, $P_0(x) =$

$3\cos(\frac{\pi x}{6})\chi_{[-3,3]}(x)$, $L = 1$

Figure 3.10: Wave Solutions with Oscillating Spreading Speed for Model (3.1) with $g(P,t)$ given by Equation (2.4)

Consider the phenology function, $g(P,t)$, as defined in equation (2.4) and parameters $D = 1$, $\theta(P) = \frac{0.9P}{1+P}$, $k(P) = 0.2 + \frac{4.5P}{13+P}$, $\alpha = 2$, $\nu = 1.3$, $\beta = 0.1$, and $P_0(x) = 3\cos(\frac{\pi x}{6})\chi_{[-3,3]}(x)$. We see that model (3.1) has wave solutions (Figure 3.10 (a)) which grow from $P_0(x)$ and spreads in both directions with an oscillating spreading speed (Figure 3.10 (b)).

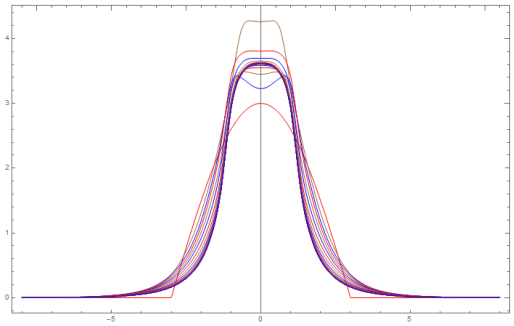

(a) Solutions $P_0(x)$ through $P_{50}(x)$ for model (3.1)

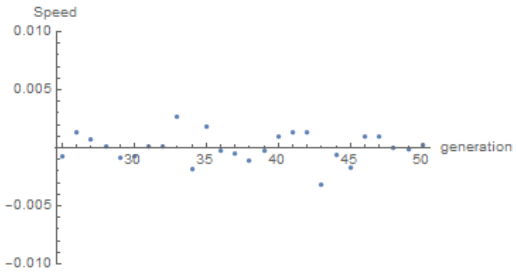

(b) Spreading speed for model (3.1)

$D = 1$, $\theta(P) = \frac{0.95P}{1+P}$, $k(P) = 0.2 + \frac{4.5P}{13+P}$, $\alpha = 2$, $\nu = 1.8$, $\beta = 0.05$, $P_0(x) = 3\cos(\frac{\pi x}{6})\chi_{[-3,3]}(x)$, $L = 1$

Figure 3.11: Nonspreading Solution for Model (3.1) with $g(P,t)$ given by Equation (2.4)

Consider the phenology function, $g(P,t)$, as defined in equation (2.4) and parameters $D = 1$, $\theta(P) = \frac{0.95P}{1+P}$, $k(P) = 0.2 + \frac{4.5P}{13+P}$, $\alpha = 2$, $\nu = 1.8$, $\beta = 0.05$, and $P_0(x) = 3\cos(\frac{\pi x}{6})\chi_{[-3,3]}(x)$. We see that solutions of model (3.1) grow from $P_0(x)$ to a stable nonspreading solution, i.e. the solution oscillates but does not spread in

time (Figures 3.11 (a) and (b)).

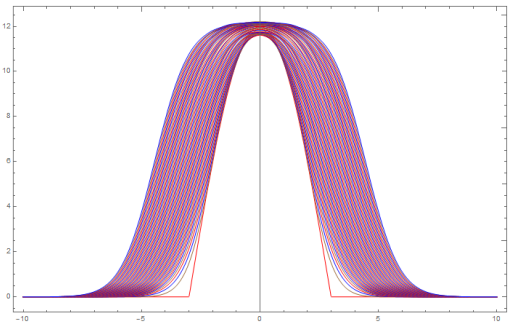

(a) Solutions $P_0(x)$ through $P_{100}(x)$ for model (3.1)

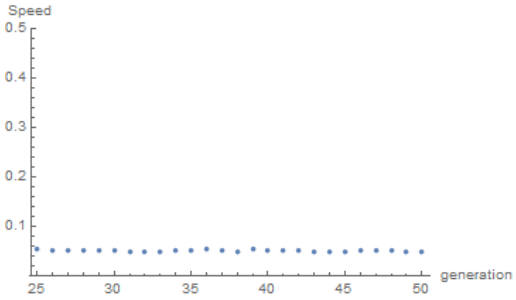

(b) Spreading speed for model (3.1)

$D = 1$, $\theta(P) = \frac{0.5P}{0.5+P}$, $k(P) = 0.5 + \frac{0.5P}{0.8+P}$, $\alpha = 12$, $\nu = 6.5$, $\beta = 0.5$, $P_0(x) = 12\cos(\frac{\pi x}{6})\chi_{[-3,3]}(x)$, $L = 1$

Figure 3.12: Wave Solution with Constant Spreading Speed for Model (3.1) with $g(P,t)$ given by Equation (2.4)

Consider the phenology function, $g(P,t)$, as defined in equation (2.4) and parameters $D = 1$, $\theta(P) = \frac{0.5P}{0.5+P}$, $k(P) = 0.5 + \frac{0.5P}{0.8+P}$, $\alpha = 12$, $\nu = 6.5$, $\beta = 0.5$, and $P_0(x) = 12\cos(\frac{\pi x}{6})\chi_{[-3,3]}(x)$. We see that model (3.1) has wave solutions (Figure 3.12 (a)) which grow from $P_0(x)$ to the carrying capacity and spreads in both directions with a constant spreading speed (Figure 3.12 (b)).

3.2.2 WHEN THE PHENOLOGY FUNCTION IS THE GAMMA DISTRIBUTION

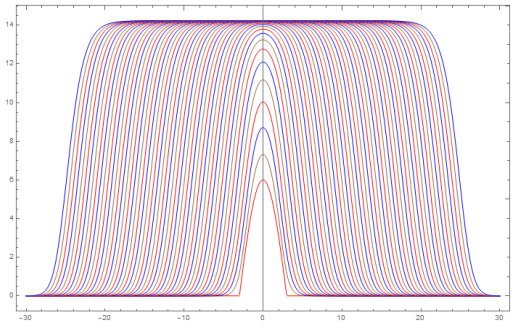

(a) Solutions $P_0(x)$ through $P_{50}(x)$ for model (3.1)

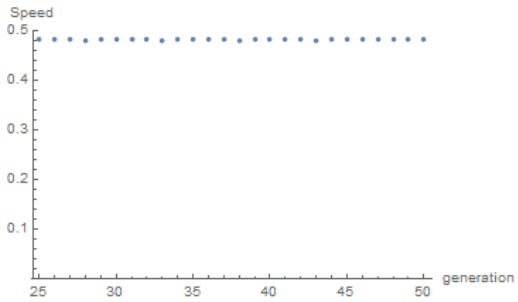

(b) Spreading speed for model (3.1)

$D = 1$, $\theta(P) = 0.5$, $k(P) = 4 - \frac{2P}{3+P}$, $\alpha = 5$, $\nu = 0.1$, $\beta = 0.2$, $P_0(x) = 6\cos(\frac{\pi x}{6})\chi_{[-3,3]}(x)$, $L = 0.01$.

Figure 3.13: Wave Solutions with Constant Spreading Speed for Model (3.1) with $g(P,t)$ given by Equation (2.7)

Consider the phenology function, $g(P,t)$, as defined in equation (2.7) and parameters $D = 1$, $\theta(P) = 0.5$, $k(P) = a - \frac{2P}{3+P}$, $\alpha = 5$, $\nu = 0.1$, $\beta = 0.2$, and $P_0(x) = 6\cos(\frac{\pi x}{6})\chi_{[-3,3]}(x)$ We see that model (3.1) has an wave solutions (Figure 3.13 (a)) which grow from $P_0(x)$ to the carrying capacity and spreads in both directions with a constant spreading speed (Figure 3.13 (b)).

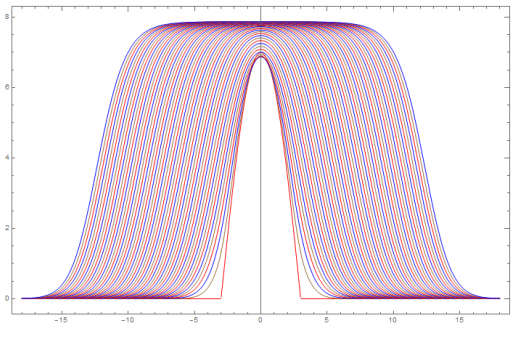

(a) Solutions $P_0(x)$ through $P_{50}(x)$ for model (3.1)

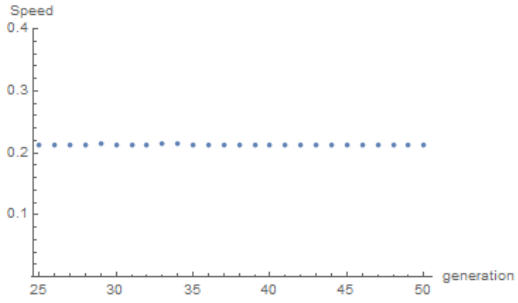

(b) Spreading speed for model (3.1)

$D = 1$, $\theta(P) = 10 - \frac{9.95P}{1+P}$, $k(P) = 1$, $\alpha = 8$, $\nu = 1$, $\beta = 0.3$, $P_0(x) = 7\cos(\frac{\pi x}{6})\chi_{[-3,3]}(x)$, $L = 0.5$.

Figure 3.14: Wave Solutions with Constant Spreading Speed for Model (3.1) with $g(P,t)$ given by Equation (2.7)

Consider the phenology function, $g(P,t)$, as defined in equation (2.7) and parameters $D = 1$, $\theta(P) = 10 - \frac{9.95P}{1+P}$, $k(P) = 1$, $\alpha = 8$, $\nu = 1$, $\beta = 0.3$, and $P_0(x) = 7\cos(\frac{\pi x}{6})\chi_{[-3,3]}(x)$. We see that model (3.1) has wave solutions (Figure 3.14 (a)) which grow from $P_0(x)$ to the carrying capacity and spreads in both directions with a constant spreading speed (Figure 3.14 (b)).

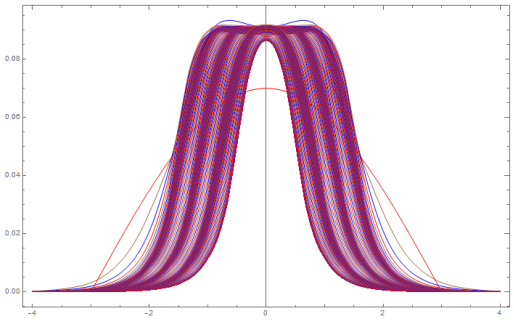

(a) Solutions $P_0(x)$ through $P_{450}(x)$ for model (3.1)

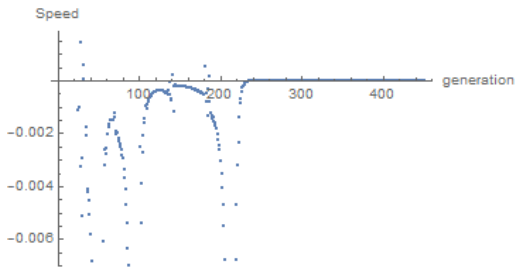

(b) Spreading speed for model (3.1)

$D = 0.5$, $\theta(P) = 0.1$, $k(P) = 1.1 + \frac{125P}{1+P}$, $\alpha = 6$, $\nu = 5$, $\beta = 5$, $P_0(x) = 0.07\cos(\frac{\pi x}{6})\chi_{[-3,3]}(x)$, $L = 0.01$.

Figure 3.15: Nonspreading Solution for Model (3.1) with $g(P,t)$ given by Equation (2.7)

Consider the phenology function, $g(P,t)$, as defined in equation (2.7) and parameters $D = 0.5$, $\theta(P) = 0.1$, $k(P) = 1.1 + \frac{125P}{1+P}$, $\alpha = 6$, $\nu = 5$, and $\beta = 5$. We see that model (3.1) has a stable nonspreading solution, i.e. the solution oscillates but does not spread in time. If we let $P_0(x) = 0.07\cos(\frac{\pi x}{6})\chi_{[-3,3]}(x)$, we see that the solutions grows above the stable attractor and slowly shrinks down to the stable nonspreading solution (it takes about 235 generations before the solution converges

to the attractor) (Figures 3.15 (a) and (b)). If we let $P_0(x) = 0.07\cos(\frac{\pi x}{6})\chi_{[-1,1]}(x)$, we see that the solutions quickly grows and converges to the stable attractor (it takes about 30 generations for the solution to converge to the attractor) (Figures 3.16 (a) and (b)).

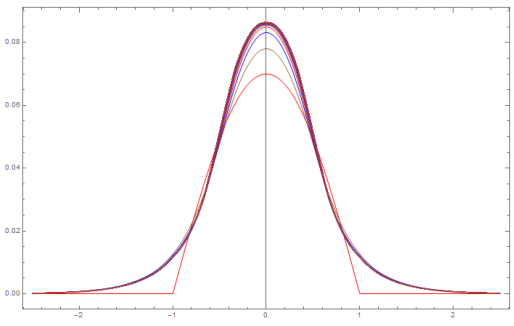

(a) Solutions $P_0(x)$ through $P_{100}(x)$ for model (3.1)

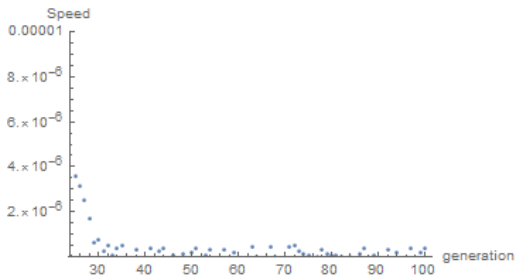

(b) Spreading speed for model (3.1)

$D = 0.5$, $\theta(P) = 0.1$, $k(P) = 1.1 + \frac{125P}{1+P}$, $\alpha = 6$, $\nu = 5$, $\beta = 5$, $P_0(x) = 0.07\cos(\frac{\pi x}{2})\chi_{[-1,1]}(x)$, $L = 0.01$.

Figure 3.16: Nonspreadng Solution for Model (3.1) with $g(P,t)$ given by Equation (2.7)

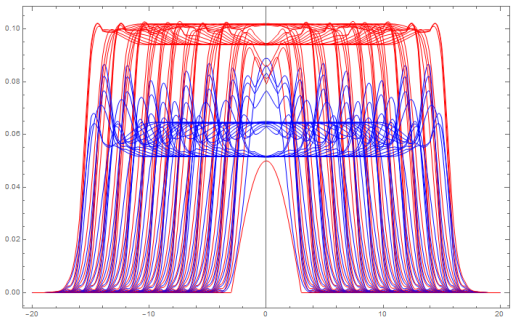

(a) Solutions $P_0(x)$ through $P_{100}(x)$ for model (3.1)

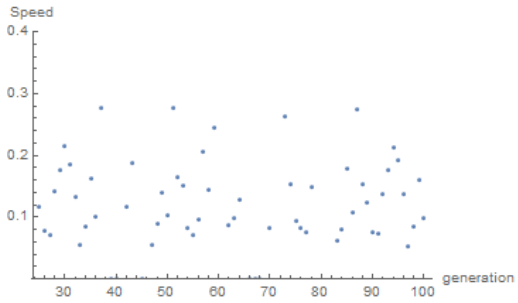

(b) Spreading speed for model (3.1)

$D = 1.5$, $\theta(P) = 0.2$, $k(P) = 1.1 + \frac{85P}{1+P}$, $\alpha = 21$, $\nu = 10$, $\beta = 6$, $P_0(x) = 0.05\cos(\frac{\pi x}{6})\chi_{[-3,3]}(x)$, $L = 0.01$.

Figure 3.17: Oscillating Wave Solutions with Chaotic Spreading Speed for Model (3.1) with $g(P,t)$ given by Equation (2.7)

Consider the phenology function, $g(P,t)$, as defined in equation (2.7) and parameters $D = 1.5$, $\theta(P) = 0.2$, $k(P) = 1.1 + \frac{85P}{1+P}$, $\alpha = 21$, $\nu = 10$, $\beta = 6$, and $P_0(x) = 0.05\cos(\frac{\pi x}{6})\chi_{[-3,3]}(x)$. We see that solutions of model (3.1) grow from $P_0(x)$ to wave solutions which oscillate around the carrying capacity (Figure 3.17 (a)) and spreads in both directions with chaotic spreading speed (Figure 3.17 (b)).

3.2.3 WHEN THE PHENOLOGY FUNCTION IS THE GENERALIZED BETA DISTRIBUTION

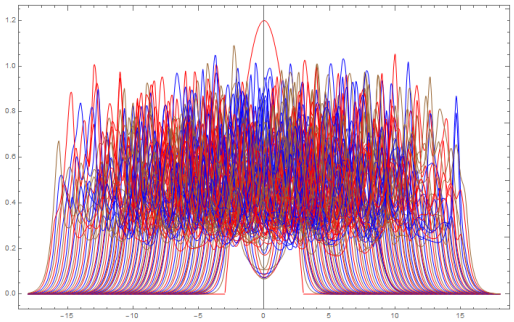

(a) Solutions $P_0(x)$ through $P_{100}(x)$ for model (3.1)

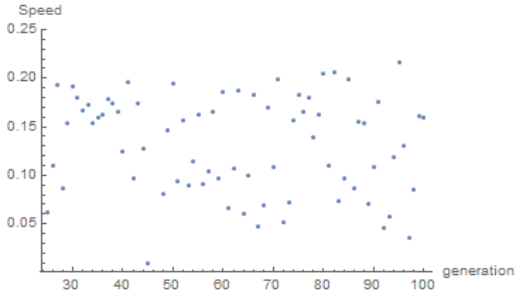

(b) Spreading speed for model (3.1)

$D = 1$, $\theta(P) = 0.5$, $k(P) = 1 - \frac{0.9P}{1+P}$, $a1 = 2$, $b1 = 0.5$, $p1 = 0.5$, $\alpha = 22$, $\nu = 10.5$, $\beta = 3$, $P_0(x) = 1.2\cos(\frac{\pi x}{6})\chi_{[-3,3]}(x)$, $L = 0.1$.

Figure 3.18: Chaotic Wave Solutions with Chaotic Spreading Speed for Model (3.1) with $g(P,t)$ given by Equation (2.8)

Consider the phenology function, $g(P,t)$, as defined in equation (2.8) and parameters $D = 1$, $\theta(P) = 0.5$, $k(P) = 1 - \frac{0.9P}{1+P}$, $a1 = 2$, $b1 = 0.5$, $p1 = 0.5$, $\alpha = 22$,

$\nu = 10.5$, $\beta = 3$, and $P_0(x) = 1.2\cos(\frac{\pi x}{6})\chi_{[-3,3]}(x)$. We see that model (3.1) has chaotic wave solutions (Figure 3.18 (a)) which grow from $P_0(x)$ and spreads in both directions with chaotic spreading speed (Figure 3.18 (b)).

CHAPTER 4
CONCLUSIONS

In this paper we showed that it is possible for density dependent phenology to cause both Allee effect and overcompensation and wave solutions with nonconstant spreading speeds. In Chapter 2, we gave integral conditions for the existence of strong Allee effects and showed that if Allee effect is present, it is caused by the density dependent phenology. We also gave a necessary conditions and a sufficient condition for the existence of a positive equilibrium for model (2.1). One thing that sets our models apart from previous models is that we only require one equation to generate the Allee effect. Most other mechanistic models that have the Allee effect require at least two equations to generate the Allee effect (e.g., two-sex models).

In Section 2.2.1, we explored the dynamics of model (2.1) when the phenology function, $g(P,t)$, was the uniform distribution (equation (2.4)). Since the uniform distribution is piecewise constant, we were able to explicitly solve model (2.1) and give the year-to-year mapping (see equation (2.5)). It was shown that model (2.1) can have a growth function that is monotone (Figures 2.2 (c) and 2.12 (c)), or has overcompensation and a cusp (Figures 2.3 (c), 2.4 (c) and (d), 2.5 (c), 2.6 (c), 2.7 (c), 2.8 (c), 2.9 (c), 2.10 (c), and 2.11 (c)). We also numerically explored how varying a parameter effected the the dynamics of model (2.1) (Figures 2.2 (a), 2.3 (a), 2.4 (a), 2.5 (a), 2.6 (a), 2.7 (a), 2.8 (a), 2.9 (a), 2.10 (a), 2.11 (a), 2.12 (a)) and effected the equilibrium points (the carrying capacity and the Allee threshold) (Figures 2.2 (b), 2.3 (b), 2.4 (b), 2.5 (b), 2.6 (b), 2.7 (b), 2.8 (b), 2.9 (b), 2.10 (b),

2.11 (b), and 2.12 (b)). It was surprising to find the models exhibiting such rich dynamics for such a simple phenology function.

In Section 2.2.2, we explored the dynamics of model (2.1) when the phenology function, $g(P,t)$, was the gamma distribution (equation (2.7)). It was shown that model (2.1) can have a monotone growth function (Figures 2.14 (c) and 2.15 (c)) or a smooth growth function with overcompensation (Figures 2.16 (c) and 2.17 (c)). We also numerically explored how varying a parameter effected the dynamics of the model (Figures 2.14 (a), 2.15 (a), 2.16 (a), and 2.17 (a)) and effected the equilibrium points (the carrying capacity and the Allee threshold) (Figures 2.14 (b), 2.15 (b), 2.16 (b), and 2.17 (b)).

In Section 2.2.3, we explored the dynamics of model (2.1) when the phenology function, $g(P,t)$, was the generalized beta distribution (equation (2.8)). We showed that model (2.1) can have a growth function with overcompensation and a cusp (Figure 2.19 (c)). We also numerically explored how varying a parameter effected the dynamics of model (2.1) (Figure 2.19 (a)) and effected the equilibrium points (the carrying capacity and the Allee threshold) (Figure 2.19 (b)).

In Chapter 3, we introduced the spatial model (model (3.1)) associated with model (2.1) if it is assumed that the adults move according to random diffusion processes. We also numerically explored the dynamics of model (3.1) for different phenology functions and showed that the model can exhibit wave solutions with nonconstant spreading speeds.

In Section 3.2.1, we explored the dynamics of model (3.1) when the phenology function, $g(P,t)$, was the uniform distribution (equation (2.4)). We showed

that the model can exhibit wave (Figures 3.1 (a), 3.10 (a), and 3.12 (a)), oscillating wave (Figures 3.2 (a), 3.3 (a), and 3.4 (a)), chaotic wave (Figures 3.5 (a), 3.6 (a), 3.7 (a), and 3.8 (a)), and nonspreading solutions (Figures 3.9 (a) and 3.11 (a)). It was also shown that these solutions can spread with a constant (Figures 3.1 (b), 3.2 (b), 3.3 (b), 3.4 (b), and 3.12 (b)) or oscillating (Figures 3.5 (b), 3.6 (b), 3.7 (b), 3.8 (b), and 3.10 (b)) spreading speeds.

In Section 3.2.2, we explored the dynamics of model (3.1) when the phenology function, $g(P,t)$, was the gamma distribution (equation (2.7)). We showed that the model can exhibit wave (Figures 3.13 (a) and 3.14 (a)), oscillating wave (Figure 3.17 (a)), and nonspreading (Figures 3.15 (a) and 3.16 (a)). It was also shown that these solutions can spread with constant (Figures 3.13 (b) and 3.14 (b)) or chaotic (Figure 3.17 (b)) spreading speeds.

In Section 3.2.3, we explored the dynamics of model (3.1) when the phenology function, $g(P,t)$, was the generalized beta distribution (equation (2.8)). We showed that the model can exhibit chaotic wave solutions (Figure 3.18 (a)) that spreads with a chaotic spreading speed (Figure 3.18 (b)).

There are many possible extensions of our models. It would be interesting to investigate the what would happen if the assumption on movement in model (2.1) was changed from movement and growth take place simultaneously to movement and growth take place in nonoverlapping stages. Changing this assumption on movement and assuming that growth was modeled by model (2.1) would lead to an integrodifference equation of the form

$$P_{n+1}(x) = \int_{-\infty}^{\infty} k(x-y) f(P_n(y)) dy$$

where $k(x)$ is the dispersal kernal and $f(P_n(x))$ is the solution map of model (2.1).

It would also be interesting to investigate how the dynamics changed if a stage structure was added to model (2.1) (e.g., adding at least one juvenile stage). This would lead to a model of the form

$$\begin{aligned} A_t &= m(t)J - \nu_1 A - \beta_1 A^2, & A(P_n, 0) = 0 \\ J_t &= \alpha g(P_n, t)P_n - (\nu_2 + m(t))J - \beta_2 E^2 & J(P_n, 0) = 0 \\ P_{n+1} &= A(P_n, 1). \end{aligned}$$

where $m(t)$ is a phenology kernel accounting for the conversion of juveniles to adults.

Another interesting modification to model (2.1) would be to remove the assumption that any unhatched eggs die at the end of the year and see how this changes the dynamics of the model. This would lead to an equation of the form

$$\begin{aligned} A_t &= (\alpha P_n^1 + P_n^2 + \dots)g(P_n, t) - \nu A - \beta A^2, \quad A(P_n, 0) = 0 \\ P_{n+1}^1 &= A(P_n, 1). \\ P_{n+1}^2 &= \sigma_1 P_n^1. \\ &\vdots \\ P_{n+1}^k &= \sigma_{k-1} P_n^{k-1} \\ &\vdots \end{aligned}$$

where P_n^k is the number of k-year-old eggs in year n and σ_k is the probability that a k-year-old egg becomes a $(k+1)$-year-old egg.

REFERENCES

S. Abubaker. Effect of plant density on flowering date, yield and quality attribute of bush beans (phaseolus vulgaris l.) under center pivot irrigation system. *American Journal of Agricultural and Biological Sciences*, 3 (4):666–668, 2008.

L. Berec, E. Angula, and F. Courchamp. Multiple allee effects and population management. *Trends Ecol. Evol.*, 22:185–191, 2007.

D. Boukal and L. Berec. Single-species models of the allee effect: Extinction boundaries, sex ratios and mate encounters. *J. Theor. Biol.*, 218:375–394, 2002.

J. M. Calabrese and W. F. Fagan. Lost in time, lonely, and single: reproductive asynchrony and the allee effect. *American Naturalist*, 164:25–37, 2004.

J. M. Calabrese, L. Ries, S.F. Matter, J. Auckland, J. Roland, D.M.. Debinski, and W.F. Fagan. Reproductive asynchrony in natural butterfly populations and its consequences for female matelessness. *Journal of Animal Ecology.*, 77:746–756, 2008.

F. Courchamp, G. Rasmussen, and D. Macdonald. Small pack size imposes a trade-off between hunting and pup-gaurding in the painted hunting dog lycaon pictus. *Behavioral Ecology*, 13(1):11–19, 2002.

F. Courchamp, L. Berec, and J. Gascoigne. Allee effects in ecology and conservation. *Oxford University Press, London*, 2008.

H. G. Davis, C. M. Taylor, J. G. Lambrinos, and D. R. Strong. Pollen limitation

causes an allee effect in a wind-pollinated invasive grass (spartina alterniflora). *Proc. Natl. Acad. Sci. USA*, 101:13804–13807, 2004.

H. Eskola and K. Parvinen. On the mechanistic underpinning of discrete-time population models with allee effect. *Theoretical Population Biology*, 72:41–51, 2007.

H. Eskola and K. Parvinen. The allee effect in mechanistic models based on inter-individual interaction processes. *Bull. Math. Biol.*, 72:184–207, 2010.

J. Gascoigne, L. Berec, S. Gregory, and F. Courchamp. Dangerously few liaisons: a review of mate-finding allee effects. *Population Ecology*, 51:355–372, 2009.

D. R. Gray. The gypsy moth life stage model: landscape-wide estimates of gypsy moth establishment using a multi-generational phenology model. *Ecological Modelling*, 176:155–171, 2004.

M. J. Groom. Allee effects limit population viability of an annual plant. *The American Naturalist*, 151:487–496, 1998.

D. M. Johnson, A. M. Liebhold, P. C. Tobin, and O. N. Bjrnstad. Allee effects and pulsed invasion by the gypsy moth. *Nature*, 44:361–363, 2006.

M. A. Lewis and B. Li. Spreading speed, traveling waves, and minimal domain size in impulsive reaction-diffusion models. *Bull. Math. Biol.*, 74:2383–2402, 2012.

J. A. Logan and J. A. Powell. Ghost forests, global warming, and the mountain pine beetle (coleoptera: Scolytidae). *American Entomologist*, 47:160, 2001.

H. J. Lynch, M. Rhainds, J. M. Calabrese, S. Cantrell, C. Cosner, and W. F. Fagan. How climate extremes not means define a species? geographic range boundary via a demographic tipping point. *Ecological Monographs*, 84:134–149, 2014.

L. Mailleret and V. Lemesle. A note on semi-discrete modelling in the life sciences. *Philosophical Transactions of the Royal Society A-mathematical and Engineering*, 1908:4779–4799, 2009.

G. Otto and B. Li. Nonspreading solutions in an integro-difference model incorporating allee and overcompensation effects. *(submitted)*, 2017.

G. Otto, S. Bewick, B. Li, and W. F. Fagan. How phenological variation affects species spreading speeds. *Bull. Math. Biol.*, 80:1476–1513, 2018.

T. D. Paine, K. F. Raffa, and T. C. Harrington. Interactions among scolytid bark beetles, their associated fungi, and live host conifers. *Annual review of entomology*, 42:179–206, 1997.

M. Rhainds and W. F. Fagan. Broad-scale latitudinal variation in female reproductive success contributes to the maintenance of a geographic range boundary in bagworms (lepidoptera: Psychidae). *PLOS One*, 5:e14166, 2010.

D. Rinella, M. Wipfli, C. Stricker, R. Heintz, and M. Rinella. Pacific salmon (oncorhynchus spp.) runs and consumer fitness: growth and energy storage in stream-dwelling salmonids increase with salmon spawner density. *Canadian Journal of Fisheries and Aquatic Sciences*, 69(1):73–84, 2012.

C. Robinet, A. Liebhold, and D. Gray. Variation in developmental time affects mating success and allee effects. *Oikos*, 116:1227–1237, 2007.

C. Robinet, D. R. Lance, K. W. Thorpe, K. S. Onufrieva, P. C. Tobin, and A. M. Liebhold. Dispersion in time and space affect mating success and allee effects in invading gypsy moth populations. *The Journal of Animal Ecology*, 77:966–973, 2008.

J. Schmitt, J. Eccleston, and D.W. Ehrahardt. Density-dependent flowering phenology, outcrossing, and reproduction in impatiens capenis. *Oecologia*, 72:341–347, 1987.

P. C. Tobin, S. L. Whitmire, D. M. Johnson, O. N. Bjrnstad, and A. M. Liebhold. Invasion speed is affected by geographical variation in the strength of allee effects. *Ecology Letters*, 10:36–43, 2007.

J. A. Walter, M. S. Meixler, T. Mueller, W. F. Fagan, P. C. Tobin, and K. J. Haynes. How topography induces reproductive asynchrony and alters gypsy moth invasion dynamics. *Journal of Animal Ecology*, 84:188–198, 2015.

N. L. Ward and G. J. Masters. Linking climate change and species invasion: an illustration using insect herbivores. *Global Change Biology*, 13:1605–1615, 2007.

APPENDIX

A.1 LEMMAS

We begin with some lemmas that are need to prove our main result.

LEMMA A.1.

For model (2.1)*, A(0,t)=0*

Proof.

Setting $P_n = 0$ in model (2.1) we have

$$\begin{aligned} A_t &= -\nu A - \beta A^2, \quad u(0) = 0 \\ P_{n+1} &= A(0,1) \end{aligned} \tag{A.1}$$

Note that $A = 0$ is a solution of (A.1), this solution is unique due to the Picard-Lindelof theorem. We next provide an alternate was to show that $A = 0$ is the unique solution of (A.1). If $u \neq 0$ then we can divide by A^2 and make the substitution $y = A^{-1}$. This yields the equation

$$y' - \nu y = \beta \tag{A.2}$$

Solving (A.2) gives us $A^{-1} = y = \frac{-\beta}{\nu} + ce^{\nu t}$.

And hence, $A = \frac{1}{c\nu e^{\nu t} - \frac{\beta}{\nu}}$.

Solving for c

$0 = A(0,0) = \frac{1}{c\nu - \frac{\beta}{\nu}} \neq 0 \implies$ no solution.

Hence $A = 0$ is the only solution. □

LEMMA A.2.

In model (2.1), $\frac{\partial}{\partial P} A(P,0)\Big|_{P=0} = 0$

Proof. recall that $A(P,0) = 0 \ \forall P$ and $A(0,t) = 0 \ \forall t \geq 0$

$$\begin{aligned}\frac{\partial}{\partial P} A(P,0)\Big|_{P=0} &= \lim_{h\to 0} \frac{A(h,0) - A(0,0)}{h} \\ &= \lim_{h\to 0} \frac{0}{h} \\ &= 0\end{aligned}$$

□

LEMMA A.3.

In model (2.1), $\frac{\partial}{\partial P} A(P,t)\Big|_{P=0} = \alpha e^{-\nu t} \int_0^t g(0,s) e^{\nu s} ds$

Proof. Taking the derivative of (2.1) with respect to P yields:

$$\frac{\partial}{\partial P} A_t = \alpha g(P,t) + \alpha P \frac{\partial}{\partial P} g(P,t) - \nu \frac{\partial}{\partial P} A - 2\beta A \frac{\partial}{\partial P} A \qquad A(P,0) = 0$$

solving this for $\frac{\partial}{\partial P} A$, we get:

$$\begin{aligned}\frac{\partial}{\partial P} A(P,t) =& \alpha e^{-\int_0^t (\nu + 2\beta A(P,\tau)) d\tau} \int_0^t (g(P,\tau) \\ &+ P \frac{\partial}{\partial P} g(P,\tau)) e^{\int_0^\tau (\nu + 2\beta A(P,\tau)) dr} d\tau + \left(\frac{\partial}{\partial P} A(P,0) \right) e^{-\int_0^t (\nu + 2\beta A(P,\tau)) d\tau}\end{aligned}$$

evaluating at $P = 0$ yields:

$$\frac{\partial}{\partial P} A(P,t)\Big|_{P=0} = \alpha e^{-\nu t} \int_0^t g(0,\tau) e^{\nu \tau} d\tau$$

□

A.2 PROOF OF THEOREM 2.1

Recall model (2.1),

$$A_t = \alpha g(P_n, t)P_n - \nu A - \beta A^2, \quad A(P_n, 0) = 0$$

$$P_{n+1} = A(P_n, 1).$$

Solving model (2.1) we have,

$$A(P_n, t) = \alpha P_n e^{-\int_0^t (\nu+\beta A(P_n,s))ds} \int_0^t g(P_n, s) e^{\int_0^s (\nu+\beta A(P_n,r))dr} ds,$$

which gives the (implicit) year-to-year mapping

$$\begin{aligned} P_{n+1} &= A(P_n, 1) \\ &= \alpha P_n e^{-\int_0^1 (\nu+\beta A(P_n,t))dt} \int_0^1 g(P_n, t) e^{\int_0^t (\nu+\beta A(P_n,s))ds} dt \\ &= \alpha P_n \int_0^1 g(P_n, t) e^{-\int_t^1 (\nu+\beta A(P_n,s))ds} dt \\ &:= f(P_n) \end{aligned} \tag{A.3}$$

Recall that a model of the form $x_{n+1} = f(x_n)$ has Allee effect if $f''(0) > 0$ and the Allee effect is strong if $f'(0) < 1$.

$$\begin{aligned} f'(P) =& \alpha \int_0^1 g(P, t) e^{-\int_t^1 (\nu+\beta A(P,s))ds} dt + \alpha P \int_0^1 \frac{\partial}{\partial P}[g(P, t)] e^{-\int_t^1 (\nu+\beta A(P,s))ds} dt \\ & - \alpha P \int_0^1 g(P, t) e^{-\int_t^1 (\nu+\beta A(P,s))ds} \frac{\partial}{\partial P} \left[\int_t^1 (\nu + \beta A(P, s))ds \right] dt \end{aligned}$$

$$
\begin{aligned}
f''(P) =& 2\alpha \int_0^1 \frac{\partial}{\partial P}[g(P,t)]e^{-\int_t^1(\nu+\beta A(P,s))ds}dt \\
&- 2\alpha \int_0^1 g(P,t)e^{-\int_t^1(\nu+\beta A(P,s))ds}\frac{\partial}{\partial P}\left[\int_t^1(\nu+\beta A(P,s))ds\right]dt \\
&+ \alpha P \int_0^1 \frac{\partial^2}{\partial P^2}[g(P,t)]e^{-\int_t^1(\nu+\beta A(P,s))ds}dt \\
&- 2\alpha P \int_0^1 \frac{\partial}{\partial P}[g(P,t)]e^{-\int_t^1(\nu+\beta A(P,s))ds}\frac{\partial}{\partial P}\left[\int_t^1(\nu+\beta A(P,s))ds\right]dt \\
&- \alpha P \int_0^1 g(P,t)e^{-\int_t^1(\nu+\beta A(P,s))ds}\frac{\partial^2}{\partial P^2}\left[\int_t^1(\nu+\beta A(P,s))ds\right]dt
\end{aligned}
$$

$$
\begin{aligned}
f''(0) &= 2\alpha \int_0^1 \left(\left[\frac{\partial}{\partial P}g(P,t)\right]\Big|_{P=0}\right)e^{-(1-t)\nu}dt \\
&\quad - 2\alpha\beta \int_0^1 g(0,t)e^{-(1-t)\nu}\int_t^1\left(\frac{\partial}{\partial P}u(P,s)\right)\Big|_{P=0}dsdt \\
&= 2\alpha \int_0^1 \left(\left[\frac{\partial}{\partial P}g(P,t)\right]\Big|_{P=0}\right)e^{-(1-t)\nu}dt \\
&\quad - 2\alpha^2\beta \int_0^1 g(0,t)e^{-(1-t)\nu}\int_t^1 e^{-\nu s}\int_0^s g(0,r)e^{\nu r}drdsdt
\end{aligned}
$$

$$
f'(0) = \alpha \int_0^1 g(0,t)e^{-(1-t)\nu}dt
$$

Hence, Allee effect is present when:

$$f''(0) = 2\alpha \int_0^1 \left(\left[\frac{\partial}{\partial P} g(P,t) \right] \Big|_{P=0} \right) e^{-(1-t)\nu} dt$$
$$- 2\alpha^2 \beta \int_0^1 g(0,t) e^{-(1-t)\nu} \int_t^1 e^{-\nu s} \int_0^s g(0,r) e^{\nu r} dr ds dt > 0$$

If Allee effect is present, then the Allee effect is strong if:

$$f'(0) = \alpha \int_0^1 g(0,t) e^{-(1-t)\nu} dt < 1$$

A.3 PROOF OF PROPOSITION 2.1

Proof.

Consider the implicit map $f(P)$ as defined in (A.3). In order for a positive equilibrium of model (2.1) to exist, there must be some $P > 0$ such that $f(P) = P$.

Assume $\alpha < 1$ and note that $A(P,t) \geq 0 \ \forall \ P, t \geq 0$.

$$\begin{aligned} f(P_n) &= \alpha P_n \int_0^1 g(P_n,t) e^{-\int_t^1 (\nu + \beta A(P_n,s)) ds} dt \\ &< P_n \int_0^1 g(P_n,t) e^{-\int_t^1 (\nu + \beta A(P_n,s)) ds} dt, \qquad (\alpha < 1) \\ &\leq P_n \int_0^1 g(P_n,t) dt, \qquad \left(e^{-\int_t^1 (\nu + \beta A(P_n,s)) ds} \leq 1 \right) \\ &\leq P_n \end{aligned}$$

Hence, $\forall P > 0$, $f(P) < P$.

$$\alpha P \int_0^1 g(P,t) e^{-\int_t^1 (\nu+\beta A(P,s))ds} dt = P$$

$$\alpha \int_0^1 g(P,t) e^{-\int_t^1 (\nu+\beta A(P,s))ds} dt = 1 \tag{A.4}$$

$$\alpha \int_0^1 g(P,t) e^{-(1-t)\nu} dt \geq \alpha \int_0^1 g(P,t) e^{-\int_t^1 (\nu+\beta A(P,s))ds} dt = 1$$

Hence a necessary condition for (2.1) to have a positive equilibrium is

$$\exists P > 0 \text{ such that } \alpha \int_0^1 g(P,t) e^{-(1-t)\nu} dt \geq 1$$

□

A.4 PROOF OF PROPOSITION 2.2

Proof.

$$A_t = \alpha g(P_n,t) P_n - \nu A - \beta A^2, \qquad A(P_n,0) = 0, \qquad P_{n+1} = A(P_n,1) := f(P_n)$$

We wish to find conditions for which $f(P) = P$ has a positive solution. We assume $f'(0) < 1$ (i.e., $\alpha \int_0^1 g(0;t) e^{-(1-t)\nu} dt < 1$). Our goal is to find a $P > 0$ such that $f(P) > P$ so that $f(P) = P$ has a positive solution (note that $f'(0) < 1$ implies that $f(P) < P$ for small $P > 0$).

$\frac{A_t}{P} = \alpha g(P,t) - \nu \frac{A}{P} - \beta P \left(\frac{A}{P}\right)^2$

Let $B = \frac{A}{P}$

$B_t + \nu B = \alpha g(P,t) - \beta P B^2$

$$\left(B e^{\nu t}\right)_t = e^{\nu t} \left(\alpha g(P,t) - \beta P B^2\right) \tag{A.5}$$

Assume $\exists t_0 \in (0,1)$ such that $B(t_0) \geq 1$.

We require the following condition:

$$\alpha g(P,t) - \beta P - \nu > 0 \tag{A.6}$$

If $\exists t_1 \in (t_0, 1]$ such that $B(t_1) = 1$ and $B'(t_1) \leq 0$ we derive a contradiction:

$$\left(\frac{d}{dt}(Be^{\nu t})\right)\Big|_{t=t_1} = e^{\nu t_1}\left(\alpha g(P,t_1) - \beta P\right)$$

$$B'(t_1) = \alpha g(P,t_1) - \beta P - \nu > 0$$

(It should be noted, if $\nu \leq 0$, you could assume $\alpha g(P,t) - \beta P > 0$ and get the same contradiction).

Hence, $\forall t \in (t_0, 1]$ we have $B(t) > 1$ and thus $B(1) > 1$, $A(P,1) > P$, $f(P) > P$.

If $\forall t \in [0,1]$ $B(t) < 1$, we derive another contradiction. From (A.5)

$$\frac{d}{dt}\left(Be^{\nu t}\right) > e^{\nu t}\left(\alpha g(P,t) - \beta P\right), \qquad 0 \leq t \leq 1$$

$$Be^{\nu t} > \int_0^t e^{\nu s}\left(\alpha g(P,s) - \beta P\right) ds, \qquad 0 \leq t \leq 1$$

$$B(1) > e^{-\nu} \int_0^1 e^{\nu s}\left(\alpha g(P,s) - \beta P\right) ds > 1$$

The last inequality is from $\int_0^1 e^{-\nu s}\left(\alpha g(P,s) - \beta P\right) ds > e^{-\nu}$.

Hence, $\exists t \in [0,1]$ such that $B(t) > 1$ □

A.5 PROOF OF PROPOSITION 2.3

Recall model (2.1)

$$\begin{aligned} &A_t = \alpha g(P_n, t) P_n - \nu A - \beta A^2, \quad A(P_n, 0) = 0 \\ &P_{n+1} = A(P_n, 1). \end{aligned} \tag{A.7}$$

To obtain equation (2.5), we split model (2.1) into pieces depending on the values of $g(P,t)$, that is 0 for $0 \leq t < \theta(P)$ (if this case even exists), $\frac{1}{k(P)-\theta(P)}$ for $\theta(P) \leq t < k(P)$, and 0 for $t > k(P)$ and use the solution of one equation as the initial condition for the next equation. If $\theta(P) > 0$, then we start with the equation

$$A_t = -\nu A - \beta A^2, \quad A(P_n, 0) = 0. \tag{A.8}$$

Solving equation (A.8), we find that $A(t) = 0$ for $0 \leq t \leq \theta(P)$. Next (or if $\theta(P) = 0$), we can return to the ode in model (2.1) but modify the initial condition to $A(P, \theta(P)) = 0$. This gives us the following equation

$$A_t = \frac{\alpha P}{k(P) - \theta(P)} - \nu A - \beta A^2, \quad A(P_n, \theta(P)) = 0. \tag{A.9}$$

Solving equation (A.9), we find that $A(t) = h(t)$ for $\theta(P) \leq t \leq k(P)$, where $h(t)$ is given by equation (2.6). Now we can evaluate this solution at $t = k(P)$ to find the initial condition for the next piece of the model, that is $A(P, k(P)) = h(k(P))$. This yields the following equation

$$A_t = -\nu A - \beta A^2, \quad A(P_n, k(P)) = h(k(P)). \tag{A.10}$$

Solving equation (A.10), we find that $A(P,t) = \frac{\nu h(k(P)) e^{\nu k(P)}}{(\nu + \beta h(k(P)))e^{\nu t} - \beta h(k(P)) e^{\nu k(P)}}$ for $t \geq k(P)$. Summarizing the solutions that we found,

$$A(P,t) = \begin{cases} 0 & , 0 \leq t < \theta(P) \\ h(t) & , \theta(P) \leq t \leq k(P) \\ \dfrac{\nu h(k(P)) e^{\nu k(P)}}{(\nu + \beta h(k(P)))e^{\nu t} - \beta h(k(P)) e^{\nu k(P)}} & , t > k(P). \end{cases} \tag{A.11}$$

Now to obtain the year-to-year mapping, we evaluate the solution (A.11) at $t = 1$ (note that the first solution in solution (A.11) gets removed since $\theta(P) < 1 \; \forall P \geq 0$), which yields the map given by formula (2.5).

A.6 DERIVATION OF $\Lambda(\mu)$

Linearizing model (3.2) we get

$$\begin{aligned} A_t &= DA_{xx} + \alpha g(t) P_n - \nu A, \quad A(x,0) = 0 \\ P_{n+1}(x) &= A(x,1). \end{aligned} \tag{A.12}$$

Solving model (A.12) we get

$$A(x,t) = \alpha \int_0^t \int_{-\infty}^{\infty} \frac{1}{\sqrt{4\pi D(t-s)}} exp\left[-\frac{(x-y)^2}{4d(t-s)} - \nu(t-s) \right] P_n(y) g(s) dy ds$$

Evaluating at $t = 1$ gives the year-to-year mapping of the linear model,

$$\begin{aligned} P_{n+1}(x) &= \alpha \int_0^1 \int_{-\infty}^{\infty} \frac{1}{\sqrt{4\pi D(1-s)}} exp\left[-\frac{(x-y)^2}{4d(1-s)} - \nu(t-s) \right] P_n(y) g(s) dy ds \\ &:= L[P_n](x) \end{aligned}$$

To find $\Lambda(\mu)$, we first calculate $L[e^{-\mu x}](x)$.

$$\begin{aligned} L[e^{-\mu x}](x) &= \alpha \int_0^1 \int_{-\infty}^{\infty} \frac{1}{\sqrt{4\pi D(1-s)}} exp\left[-\frac{(x-y)^2}{4d(1-s)} - \nu(t-s) \right] exp\left[-\mu y \right] g(s) dy ds \\ &= \alpha \int_0^1 g(s) exp[-\nu(1-s)] exp[\mu^2 D(1-s) - \mu x] ds \end{aligned}$$

Hence,

$$\begin{aligned} \Lambda(\mu) &= L[e^{-\mu x}](0) \\ &= \alpha \int_0^1 g(s) e^{(\mu^2 D - \nu)(1-s)} ds \end{aligned}$$

CURRICULUM VITAE

Timothy James Pervenecki

EDUCATION

University of Louisville, Louisville, KY

Ph.D. Applied & Industrial Mathematics Expected August 2019

Area: Mathematical Biology and Differential Equations

Advisor: Professor Bingtuan Li

Dissertation: Allee effects introduced by density dependent phenology

University of Louisville, Louisville, KY

M.A. Mathematics May 2015

GPA: 3.775

University of Southern Indiana, Evansville, IN

B.S. Mathematics May 2013

Minor in Statistics

cum laude

GPA: 3.781

EXPERIENCE

University of Louisville, Louisville KY 2013 - Present

Assisted mentoring undergraduate students on research project

(Summer 2017)

Graduate Research Assistant in Mathematical Biology

(Fall 2014 - Summer 2015, Spring 2016, Spring 2018)

Graduate Teaching Assistant in Mathematics

Primary Instructor for the following courses:

- MATH 107: Finite Mathematics (Summer 2014, Spring 2017)

  A required course for some Math Education majors. Covers systems of linear equations and inequalities, algebra of sets, counting and probability theory, vectors and matrices, and applications.

- MATH 109: Elementary Statistics (Summer 2016)

  A required statistics course for Nursing majors, some education disciplines. Covers descriptive statistics, normal and binomial distributions, correlation and regression, and inferential statistics.

- MATH 111: Supplemented College Algebra (Fall 2015)

  A general education course for students struggling in mathematics. Reduced class size and extra time are giving to students in this class to help them learn the material. Covers algebraic and rational expressions and factoring; polynomial, rational, exponential, and logarithmic functions, with applications.

- MATH 151 Mathematics for Elementary Education 1 (Fall 2018)

  A required course for some Education majors. Covers problem solving and

number systems, including numeration systems, integers, rational, and real numbers, and elementary number theory.

- MATH 180: Elements of Calculus (Summer 2017, Summer 2018)

  A calculus class required for business majors and majors in the life sciences. Covers limits, derivatives, and integrals with applications.

- MATH 205: Calculus 1 (Summer 2019)

  A first course in differential and integral calculus of single variable functions.

Teaching Assistant for the following courses:

- MATH 107: Finite Mathematics (Fall 2013, Spring 2014)
- MATH 109: Elementary Statistics (Fall 2013)
- MATH 111: College Algebra (Fall 2016)
- MATH 180: Elements of Calculus (Fall 2016, Fall 2017)

University of Southern Indiana, Evansville IN 2012 - 2013

Student Grader

PUBLICATIONS

- Jobson A., Kézdy A., Pervenecki T. (submitted) On a conjecture of Szemerédi and Petruska.
- Jobson A., Kézdy A., Lehel J., Pervenecki T., Tóth G. (submitted) Petruska's question on planar convex sets.

- Pervenecki T., Bewick S., Li B., Fagan W. (in preparation) Allee effects introduced by density dependent phenology.
- Jobson A., Kézdy A., Lehel J., Pervenecki T. (in preparation) The intersection of the maximum cliques in 3-uniform hypergraphs.

ACHIEVEMENTS/AWARDS/GRANTS

- Supported by National Science Foundation Grant Fall 2014 - Summer 2015, Spring 2016
- Graduate Student Council Research Grant ($300) 2014
- University Honors List, University of Southern Indiana
- Academic Achievement Award for Mathematics, University of Southern Indiana 2013
- David W. Kinsey Scholarship 2012 - 2013
  One scholarship is awarded each year to a full-time USI math major
- Eagle Scout 2006

SERVICE

- General Education Committee Fall 2018-Present
  Mathematics Department, University of Louisville

LEADERSHIP

- Vice President December 2018-Present
  Pokémon Go - UofL Campus, University of Louisville
- Assisted mentoring undergraduate research Summer 2017
  University of Louisville

PRESENTATIONS

- "Density Dependent Phenology May Cause Allee Effect", American Mathematical Society Student Chapter Meeting, University of Louisville, Louisville, KY, November 2017
- "Density Dependent Phenology May Cause Allee Effect", Mathematics Association of America Sectional Meeting, Berea College, Berea, KY, March 2017
- "Density Dependent Phenology May Cause Allee Effect", Candidacy Exam, University of Louisville, Louisville, KY, April 2017
- "Allee Effect and Phenology", Graduate Student Seminar, University of Louisville, Louisville, KY, November 2016
- "A Reaction-Diffusion Model with Three Stages", Mathematical Biology Seminar, University of Louisville, Louisville, KY, March 2016

CONFERENCE ATTENDANCE

- Joint Mathematics Meetings, Baltimore, MD, January 2019
- Mathematics Association of America Sectional Meeting, Berea College, Berea, KY, March 2017
- Annual Mathematics Symposium, Western Kentucky University, Bowling Green, KY, November 2016
- Mathematics Association of America Sectional Meeting, Perdue University, West Lafayette, IN, October 2016
- American Mathematical Society Sectional Meeting, University of Louisville, Louisville, KY, October 2013

REFERENCES

- Dr. Bingtuan Li 502.852.6149 bing.li@louisville.edu
- Dr. Robert Powers 502.852.6103 robert.powers@louisville.edu
- Dr. André Kézdy 502.852.5986 kezdy@louisville.edu
- Dr. David Swanson 502.852.6234 david.swanson@louisville.edu